

# A data-driven framework for sparsity-enhanced surrogates with arbitrary mutually dependent randomness

Huan Lei<sup>a,1,\*</sup>, Jing Li<sup>a,1</sup>, Peiyuan Gao<sup>a</sup>, Panagiotis Stinis<sup>a,b</sup>, Nathan A. Baker<sup>a,c,\*</sup>

<sup>a</sup>*Pacific Northwest National Laboratory, Richland, WA 99352.*

<sup>b</sup>*Department of Applied Mathematics, University of Washington, Seattle, WA 98195.*

<sup>c</sup>*Division of Applied Mathematics, Brown University, Providence, RI 02912.*

---

## Abstract

The challenge of quantifying uncertainty propagation in real-world systems is rooted in the high-dimensionality of the stochastic input and the frequent lack of explicit knowledge of its probability distribution. Traditional approaches show limitations for such problems, especially when the size of the training data is limited. To address these difficulties, we have developed a general framework of constructing surrogate models on spaces of stochastic input with arbitrary probability measure irrespective of **the mutual dependencies between individual components of the random inputs** and the analytical form. The present *Data-driven Sparsity-enhancing Rotation for Arbitrary Randomness* (DSRAR) framework includes a **data-driven construction of multivariate polynomial basis for arbitrary mutually dependent probability measures** and a sparsity enhancement rotation procedure. This sparsity-enhancing rotation method was initially proposed in our previous work [1] for Gaussian density distributions, which may not be feasible for non-Gaussian distributions due to the loss of orthogonality after the rotation. To remedy such difficulties, **we developed a new data-driven approach to construct orthonormal polynomials for arbitrary mutually dependent randomness, ensuring the constructed basis** maintains the orthogonality/near-orthogonality with respect to the density of the rotated random vector, **where directly applying the regular polynomial chaos including arbitrary polynomial chaos (aPC)** [2] shows limitations due to the assumption of the mutual independence between the components of the random **inputs**. The developed DSRAR framework leads to accurate recovery, with only limited training data, of a sparse representation of the target functions. The effectiveness of our method is demonstrated in challenging problems such as partial differential equations and realistic molecular systems **within high-dimensional ( $O(10)$ ) conformational spaces** where the underlying density is implicitly represented by a large collection of **sample data**, as well as systems with explicitly given non-Gaussian probabilistic measures.

**Keywords:** data-driven, arbitrary randomness, mutual dependence, compressed sensing, sparsity enhancement, uncertainty quantification

---

\*Corresponding author

Email addresses: [huan.lei@pnnl.gov](mailto:huan.lei@pnnl.gov) (Huan Lei), [nathan.baker@pnnl.gov](mailto:nathan.baker@pnnl.gov) (Nathan A. Baker)

<sup>1</sup>The first two authors contributed equally

## 1. Introduction

A fundamental problem in uncertainty quantification (UQ) [3] is to calculate the statistical properties of a quantity of interest (QoI) due to various sources of randomness, e.g., numerical simulations subject to uncertain parameters, initial conditions and/or boundary conditions, as well as experimental measurements in the presence of material heterogeneity, thermal fluctuations. Such sources of uncertainty are usually characterized by high-dimensional random variables whose probability measures can be either discrete or continuous. In real-world systems, there are usually two crucial challenges to accurately quantify the propagation of the randomness from the input to the system response. The first challenge comes from the high-dimensionality of the random inputs. For such systems, limited computational resources often motivates further dimensionality reduction [4]. However, it is often non-trivial to accurately transfer the high-dimensional random space into a low-dimensional random space. This results in the numerical intractability of quantifying the uncertainty of the QoI from training data of limited size. The second challenge arises from frequent dependencies and arbitrary distribution of the random inputs. Typically, random inputs are represented by random vectors with mutually independent components. For realistic systems, the underlying distribution of the inputs can often involve dependencies that cannot be ignored (e.g., see molecule systems in Ref. [5] and Sec. 4.4). Moreover, the input distribution could be even unknown and thus we may only have access to it implicitly through a collection of samples. This creates further numerical obstacles in characterizing the random inputs as well as their effect on the system response. In the current work, we present a *Data-driven Sparsity-enhancing Rotation for Arbitrary Randomness* (DSRAR) framework for dealing with all of the aforementioned challenges. While we focused on numerical experiments in the present study, the developed framework can be also applied to UQ in experimental studies.

In practice, a straightforward and robust approach is the Monte Carlo (MC) method, which involves collecting a large number of samples of the random inputs from their distribution, evaluating the QoI at each sample point, and then obtaining the statistical properties (mean, variance, sensitivity indices, probability density function, probability of a certain event etc.) of the QoI. Unfortunately, to get an accurate estimate, the MC method requires a large number of simulations due to its slow convergence rate [6, 7]. Furthermore, for large or complex systems, even a single instance of these simulations may require very large computational resources. Under such circumstances, the computational cost of MC method can become extremely large. Several approaches have been developed to alleviate such difficulties. For instance, sampling approaches such as multilevel-MC [8, 9, 10] and multifidelity-MC [11, 12] have been designed to optimize the computational load when samples of the QoI are available at hierarchical levels of accuracy; sampling approaches like quasi-MC [13, 14, 15] and Latin Hypercube sampling [16, 17, 18], have been designed to accelerate convergence. However, when the underlying distribution of the inputs is arbitrary and not explicitly given, the latter two sampling strategies may lose their advantage if it is not straightforward to generate quasi-random sequences

35 following the underlying distribution.

An alternative approach approximates the QoI via constructing the surrogate model of the random inputs and then calculates the statistics of the QoI analytically or numerically. Among such approaches, the most popular are the Gaussian Process [19, 20, 21], and the polynomial chaos expansion originally introduced by Wiener [22], applied to UQ by Ghanem [23] and extended to the generalized polynomial chaos (gPC) expansion by Xiu [24]. The Gaussian Process (GP) is a stochastic process which approximates the values of the QoI at every finite sets of sample point as multivariate Gaussian random vectors. The flexibility of the mean and covariance functions enables GP to characterize a wide range of function behavior with broad applications on UQ [21, 25, 26, 27, 28]. The gPC expansion approximates the QoI by a set of simple basis functions. It is known to be a *mathematically optimal* approximation of the QoI when the basis functions are chosen to be orthogonal with respect to the probability measure of the random inputs. This approach has been demonstrated for diverse applications in UQ [29, 30, 31, 32, 33, 34, 35, 36] due to its spectral convergence under certain situations. In this study, we focus on the approach developed based on gPC and we refer to previous publications [37, 38, 39, 40] (and the references therein) for comparative studies of the two approaches.

50 In principle, if the orthogonal polynomial type and the corresponding random variables are determined, both intrusive and non intrusive methods can be used to evaluate the coefficients of the expansion. For example, stochastic collocation, based on tensor products of one-dimensional quadrature rules, is often employed when dimensionality is small [41, 42, 43], with the number of basis functions given by  $(p+d)!/p!d!$ , where  $p$  is polynomial order and  $d$  is the dimension. However, as the dimension increases, the number 55 of quadrature points needed for the tensor product rule increases exponentially. To mitigate this issue, sparse grid and adaptive collocation methods have been proposed to deal with moderate dimensionality [42, 44, 45, 46, 47, 48, 49]. When the dimension of the random inputs is large, none of the above collocation methods is feasible. In the case of a limited number of available simulations and large dimensionality, compressed sensing (CS) approaches have been used to construct sparse polynomial approximations of the 60 QoI [50, 51, 52, 53, 54, 55, 56, 57, 58, 59, 60, 61, 62]. Finally, we note that gPC (including extensions such as arbitrary polynomial chaos [2]), in its current form, can only handle random vector with independent identically distributed (i.i.d.) components in standard types (uniform, Gaussian, gamma, beta, etc.). For other distributions, a pre-processing step is required to transform the original random variables into i.i.d. random variables of standard types. In general, these transformations are highly nonlinear which result in 65 the final QoI function approximation to be a high-degree polynomial in order to maintain accuracy.

The methods discussed above rely on the *explicit* knowledge of the underlying probability measures and/or the assumption of mutual independence between the components of the random inputs. However, such assumptions on the random inputs can be quite restrictive for realistic applications. One such example

is the UQ for molecular system properties QoIs due to conformational fluctuations [63]. For such systems,  
 70 the random inputs are the various conformational states (i.e., the instantaneous structure) of the molecule.  
 The underlying distribution is determined by the free energy function of the system, which is essentially  
 the multi-dimensional marginal density distribution with respect to the (Boltzmann) distribution of the  
 full Hamiltonian system. Unfortunately, numerical evaluation of the free energy function is a well-known  
 challenging problem. Although various sampling strategies have been developed [64, 5, 65], the explicit  
 75 free energy function is usually unknown for dimensions greater than 4. In practice, the underlying density  
 is only known implicitly through a large collection of the molecule conformational states obtained from  
 experiments or simulated trajectories. Another commonly encountered example arises in our recent work [1]  
 on constructing sparse representations of a QoI based on CS. Inspired by the active subspace method [66],  
 we proposed a method to enhance the sparsity of polynomial expansion in terms of a new random vector  
 80 via unitary rotation of the original random vector. For i.i.d. Gaussian random inputs, the new random  
 vector retains the same distribution. However, for non-Gaussian random inputs, which are more realistic for  
 applications, the new random vector does not retain the mutual independence even if the original random  
 vector elements are i.i.d.

For problems with non-Gaussian random inputs, the traditional approach is to cast the available statistics  
 85 into a family of standard distributions and then to apply the gPC techniques discussed above. Gaussian  
 mixture models, due to their flexibility, are broadly employed to approximate the distribution of the data.  
 With the distribution approximated, a gPC expansion of the QoI can be constructed for each Gaussian  
 component. The statistical properties of the QoI are derived by combining the statistical properties of all  
 components [67, 68]. However, there are two drawbacks of the Gaussian mixture approach: (i) it lacks one-  
 90 to-one correspondence between one instance of random inputs and the approximated function evaluation, (ii)  
 it is difficult to determine an appropriate and accurate probability density approximation when the dimension  
 is larger than one. Copulas have been employed to treat dependent probabilistic models for surrogate  
 construction in [69]. Zabararas [70] has established a graph-based approach to factorize the joint distribution  
 into a set of conditional distributions based on the dependence structure of the variables. Alternatively,  
 95 several studies have been devoted to constructing orthogonal polynomial bases using the moments of the  
 random variables. Orthogonal polynomial chaos for random vectors with independent components of arbitrary  
 measure was proposed in [2, 71, 72, 73, 74]. Ahlfeld investigated the quadrature rule of this arbitrary  
 polynomial chaos (aPC) and proposed a sparse quadrature rule for the integration which can facilitate the  
 evaluation of the expansion coefficients [75]. However, those quadrature rules of arbitrary polynomial chaos  
 100 again assume *the components of the random inputs are mutually independent.*

In this paper, we develop a general UQ framework for constructing surrogate models via DSRAR *irre-  
 spective of possible mutual dependencies between the random input components.* This approach is different

from the aforementioned studies based on polynomial chaos expansions and, therefore, can be particularly useful for realistic systems where the input distributions can be non-standard or unknown analytically. The  
105 key idea is a data-driven approach for basis construction, consisting of multivariate orthonormal *polynomials for arbitrary mutually dependent* (amdP), coupled with the previously developed rotation-based sparsity enhancement approach [1]. This can be viewed a special case of the present method when the random inputs are from a Gaussian distribution. When the size of the training set is limited, the method can recover the expansion coefficients by CS, under the assumption that there exists a sparse representation of surrogate model.  
110 As we will show, directly employing a regular polynomial basis and/or the sparsity enhancement rotation on the random input may result in large recovery error due to the violation of orthogonality for non-standard density distributions. The procedure of data-driven basis construction described in the present study retains proper orthogonality with respect to the associated random inputs and therefore ensures more accurate recovery. In this sense, the present method takes advantage of both the orthonormal basis expansion and the  
115 enhanced sparsity of the expansion coefficients. The method deals with two situations widely encountered in real-world applications: (I) probability measures that are implicitly represented by a large collection of samples and (II) non-Gaussian probability measures with explicit (analytical) forms. For the first situation, we construct orthonormal polynomial bases with respect to discrete measures on the sample set. Besides the exact orthonormal basis, we also propose a heuristic method to construct a *near-orthonormal* basis, which  
120 yields a smaller basis bound than the exact orthonormal basis and results in more accurate recovery of the sparse representation. For the second situation, we construct the orthonormal basis when the quadrature rules for polynomial integration are known. This construction is especially well suited to random variables obtained from sparsity enhancement of non-Gaussian distributions.

The paper is organized as follows. In Section 2, we present the problem setup and briefly review preliminary background on multivariate orthogonal polynomials and compressed sensing. In Section 3, we present the DSRAR framework by first introducing the methods to construct data-driven orthonormal amdP basis. When the underlying density is implicitly represented by a large collection of random input samples, we propose a heuristic approach to construct a near-orthonormal basis along with some heuristics on the advantage over an exactly orthonormal basis. Then we introduce the rotation-based sparsity enhancement method and  
125 provide algorithmic details on how to combine the data-driven basis construction and sparsity enhancement rotation. In Section 4, we demonstrate the developed framework in a realistic molecular system fluctuating in a high-dimensional conformational space ( $O(10)$ ) as well as partial differential equations (PDEs) with arbitrary randomness where the underlying distributions are either explicitly known or implicitly represented by a large collection of samples. Concluding remarks and directions for future work are provided in Section 5.

### 2.1. Approximation with orthogonal polynomials

We begin with a few facts about multivariate orthogonal polynomials [76]. Let  $\Pi^d$  be the set of polynomials in  $d$  variables on  $\mathbb{R}^d$ . Polynomials in  $\Pi^d$  are naturally indexed by the multi-indices set  $\mathbb{N}_0^d$ . For  $\boldsymbol{\alpha} = (\alpha_1, \dots, \alpha_d) \in \mathbb{N}_0^d$  and  $\mathbf{z} = (z_1, \dots, z_d)$ , a monomial  $z^\alpha$  is defined by  $\mathbf{z}^\alpha = z_1^{\alpha_1} \cdots z_d^{\alpha_d}$  and the degree of  $\mathbf{z}^\alpha$  is defined by  $|\boldsymbol{\alpha}| = \alpha_1 + \cdots + \alpha_d$ . From now on, without confusion,  $|\cdot|$  operating on a [multi-index](#)  $\boldsymbol{\alpha}$  denotes the  $\ell_1$  norm of  $\boldsymbol{\alpha}$  while  $|\cdot|$  operating on a set  $T$  denotes the cardinality of  $T$ . The degree of a polynomial is defined by the largest degree of its monomial terms. Then the space of polynomials of degree at most  $p$  is defined by

$$\Pi_p^d := \text{span}\{\mathbf{z}^\alpha : |\boldsymbol{\alpha}| \leq p, \boldsymbol{\alpha} \in \mathbb{N}_0^d\} \text{ and } \dim \Pi_p^d = \binom{p+d}{p}. \quad (2.1)$$

If we equip  $\mathbb{R}^d$  with a probability measure  $\rho$ , then we can define an inner product on  $\Pi^d$ ,

$$\langle f, g \rangle_\rho = \int_{\mathbb{R}^d} fg \, d\rho \quad f, g \in \Pi^d. \quad (2.2)$$

$f$  and  $g$  are said to be orthogonal with respect to  $\rho$  if  $\langle f, g \rangle_\rho = 0$ . Given such an inner product, and an order of the set  $\mathbb{N}_0^d$ , we can apply the Gram-Schmidt process on the ordered set  $\{\mathbf{z}^\alpha : \boldsymbol{\alpha} \in \mathbb{N}_0^d\}$  to generate a sequence of orthogonal polynomials. We will revisit this construction in Section 3.1. When  $d > 1$ , there 140 is no natural order among monomials. As a result, multivariate orthogonal polynomials are, in general, not uniquely determined. In this paper, we choose the *graded lexicographic order* when applying the Gram-Schmidt process, that is,  $\mathbf{z}^\alpha \succ \mathbf{z}^\beta$  if  $|\boldsymbol{\alpha}| > |\boldsymbol{\beta}|$  or if  $|\boldsymbol{\alpha}| = |\boldsymbol{\beta}|$  and the first nonzero entry in the difference  $\boldsymbol{\alpha} - \boldsymbol{\beta}$  is positive.

When a simulation model is expensive to run, building an approximation of the response of the model 145 output with respect to the variations in the model input can often be an efficient approach to quantify uncertainty propagation. The polynomial approximation of a function (model)  $f(\mathbf{z}) : \mathbb{R}^d \rightarrow \mathbb{R}, d \geq 1$  where  $\mathbf{z} = (z_1, \dots, z_d) : \Omega \rightarrow \mathbb{R}^d$  is a  $d$ -dimensional random variable with associated probability measure  $\rho(\mathbf{z})$ , which is widely used due to its fast convergence when  $f(\mathbf{z})$  is analytic. In this paper, we will approximate  $f$  150 using an orthogonal polynomial basis. It is a generalization of the gPC expansion which usually deals with i.i.d. random variables.

Let  $\Psi = \{\psi_\boldsymbol{\alpha}(\mathbf{z}) : \boldsymbol{\alpha} \in \mathbb{N}_0^d\}$  be a set of orthonormal polynomial basis of  $\Pi^d$  associated with the measure  $\rho(\mathbf{z})$ , that is,

$$\int \psi_\boldsymbol{\alpha}(\mathbf{z}) \psi_\boldsymbol{\beta}(\mathbf{z}) \, d\rho(\mathbf{z}) = \delta_{\boldsymbol{\alpha}, \boldsymbol{\beta}}, \quad \boldsymbol{\alpha}, \boldsymbol{\beta} \in \mathbb{N}_0^d, \quad (2.3)$$

where  $\delta_{\alpha\beta} := \prod_{i=1}^d \delta_{\alpha_i, \beta_i}$  to be the multi-index Kronecker delta. Then the  $p$ th-degree arbitrary orthogonal polynomial expansion  $f_p(\mathbf{z})$  of function  $f(\mathbf{z})$  associated with  $\psi$  is defined as,

$$f(\mathbf{z}) \approx f_p(\mathbf{z}) := \sum_{\alpha \in \Lambda_p^d} c_\alpha \psi_\alpha(\mathbf{z}), \quad \Lambda_p^d = \{\alpha \in \mathbb{N}_0^d : |\alpha| \leq p\}, \quad (2.4)$$

where  $c_\alpha$  is the coefficient to be evaluated. Using an ordering of the orthonormal polynomial basis, we can change (2.4) into the following single index version

$$f_p(\mathbf{z}) = \sum_{\alpha \in \Lambda_p^d} c_\alpha \psi_\alpha(\mathbf{z}) = \sum_{n=1}^N c_n \psi_n(\mathbf{z}), \quad (2.5)$$

where  $N$  is the total number of basis and is given by

$$N = \dim \Pi_p^d = |\Lambda_p^d| = \binom{d+p}{p}.$$

## 2.2. Compressed sensing

Compressed sensing is a well-studied and popular approach to find sparse solutions to linear equations [77, 78, 79, 80]. In this subsection, we briefly review the theory of CS and discuss the conditions which allow accurate recovery of solutions to underdetermined linear system.

Under certain assumptions, the solution—or its approximation—can be found by the well-studied  $\ell_1$  minimization, i.e., finding the minimizer

$$\min \|\mathbf{c}\|_1 \quad \text{subject to } \mathbf{A}\mathbf{c} = \mathbf{b}, \quad (2.6)$$

155 where  $\mathbf{A} \in \mathbb{R}^{M \times N}$ ,  $\mathbf{b} \in \mathbb{R}^M$  and  $\|\mathbf{c}\|_1 = \sum_{i=1}^N |c_i|$  is the  $\ell_1$  norm of the vector  $\mathbf{c}$ .

When the data  $\mathbf{b}$  is contaminated by noise, the constraint in (2.6) is relaxed to obtain the basis pursuit denoising problem,

$$\min \|\mathbf{c}\|_1 \quad \text{subject to } \|\mathbf{A}\mathbf{c} - \mathbf{b}\|_2 \leq \sigma, \quad (2.7)$$

where  $\sigma$  is an estimate of the  $\ell_2$  norm of the noise. The optimization problems (2.6) and (2.7) can be solved with efficient algorithms from convex optimization [81].

Next we discuss the conditions for the sparse recovery of  $\mathbf{c}$ .

**Definition 2.1.** A vector  $\mathbf{c}$  is said to be  $s$ -sparse if it has at most  $s$  nonzero entries, i.e.,  $\mathbf{c}$  is supported on 160  $T \subset \{1, \dots, N\}$  with  $|T| \leq s$ .

**Definition 2.2** (Restricted isometry constant [82, 83]). For each integer  $s = 1, 2, \dots, N$  define the isometry constant  $\delta_s$  of a matrix  $\mathbf{A}$  as the smallest number such that

$$(1 - \delta_s) \|\mathbf{c}\|_2^2 \leq \|\mathbf{A}\mathbf{c}\|_2^2 \leq (1 + \delta_s) \|\mathbf{c}\|_2^2$$

holds for any  $s$ -sparse vector  $\mathbf{c} \in \mathbb{R}^N$ .

The restricted isometry constants (RICs) characterizes matrices that are nearly orthonormal. The sparse recovery is established by the following theorem.

**Theorem 2.3** (Sparse Recovery for restricted isometry property (RIP)-Matrices). *Let  $\mathbf{A} \in \mathbb{R}^{M \times N}$ . Assume that its isometry constant  $\delta_{2s}$  satisfies  $\delta_{2s} < 0.4931$ . Let  $\mathbf{c} \in \mathbb{R}^N$ , and assume noisy measurements  $\mathbf{b} = \mathbf{A}\mathbf{c} + \boldsymbol{\eta}$  are given with  $\|\boldsymbol{\eta}\|_2 \leq \sigma$ , then the minimizer  $\mathbf{c}^*$  of*

$$\min \|\mathbf{c}\|_1 \quad \text{subject to } \|\mathbf{A}\mathbf{c} - \mathbf{b}\|_2 \leq \sigma,$$

satisfies

$$\begin{aligned} \|\mathbf{c} - \mathbf{c}^*\|_2 &\leq C_1 \frac{\sigma_s(\mathbf{c})}{\sqrt{s}} + C_2 \sigma, \\ \|\mathbf{c} - \mathbf{c}^*\|_1 &\leq C_3 \sigma_s(\mathbf{c}) + C_4 \sqrt{s} \sigma. \end{aligned} \tag{2.8}$$

where constants  $C_1, C_2, C_3$  and  $C_4$  depend only on  $\delta_{2s}$ , and  $\sigma_s(\mathbf{c}) = \inf_{\mathbf{c}_s: \|\mathbf{c}_s\|_0 \leq s} \|\mathbf{c} - \mathbf{c}_s\|_1$  with  $\|\mathbf{c}_s\|_0$  indicates the number of nonzero entries of  $\mathbf{c}_s$ . In particular, if  $\mathbf{c}$  is  $s$ -sparse, then the reconstruction is exact.

*Proof.* See Rauhut and Ward [52]. □

A bounded orthonormal system has the following definition.

**Definition 2.4.**  $\{\psi_n\}, n = 1, \dots, N$  is a bounded orthonormal system, if

$$K := \sup_n \|\psi_n\|_\infty = \sup_n \sup_{\mathbf{z}} |\psi_n(\mathbf{z})| < \infty, \tag{2.9}$$

where  $K$  is called the basis bound.

These definitions allow us to establish the recoverability of (2.6) based on the RIP.

**Theorem 2.5** (RIP for bounded orthonormal systems). *Let  $\mathbf{A} \in \mathbb{R}^{M \times N}$  be the interpolation matrix with entries  $\{a_{j,n} = \psi_n(\mathbf{z}^{(j)})\}_{1 \leq n \leq N, 1 \leq j \leq M}$  (see (3.2)), where  $\{\psi_n\}$  is a bounded orthonormal system satisfying (2.9). Assume that*

$$M \geq C \delta^{-2} K^2 s \log^3(s) \log(N),$$

then with probability at least  $1 - N^{-\gamma \log^3(s)}$ , the RIC  $\delta_s$  of  $1/\sqrt{M}\mathbf{A}$  satisfies  $\delta_s \leq \delta$ . Here,  $C, \gamma > 0$  are universal constants.

*Proof.* See Rauhut and Ward [52]. □

Theorem 2.3 and Theorem 2.5 establish the sparse recoverability of the bounded orthonormal systems.

### 3. Methods

In this section, we introduce the DSRAR framework to construct surrogate model. The goal of this study is to determine, given a small set of  $M \ll N$  unstructured realizations  $\{\mathbf{z}^{(i)}\}_{i=1}^M$  and the corresponding outputs  $b = (f(\mathbf{z}^{(1)}), \dots, f(\mathbf{z}^{(M)}))^T$ , the polynomial approximation in (2.4) or (2.5) when  $f(\mathbf{z})$  has a sparse representation. This small set  $\{\mathbf{z}^{(i)}\}_{i=1}^M$  is usually called *training set* and  $M$  is the *training sample size*. There are two quantities we need to compute: (i) an appropriate orthonormal polynomial basis  $\psi$  and (ii) an interpolation-type sparse solution  $\mathbf{c} = (c_1, \dots, c_N)^T \in \mathbb{R}^N$  such that  $f_p(\mathbf{z}^{(i)}) = f(\mathbf{z}^{(i)})$  for  $i = 1, \dots, M$  with the smallest possible number nonzero  $\mathbf{c}$ . The basis construction, step (i), will be discussed in detail in Section 3.1. We can reformulate the second part as the following constrained optimization problem,

$$\min \|\mathbf{c}\|_0 \quad \text{subject to } \mathbf{A}\mathbf{c} = \mathbf{b}, \quad (3.1)$$

where  $\|\mathbf{c}\|_0$  indicates the number of nonzero entries of  $\mathbf{c}$  and  $\mathbf{A} \in \mathbb{R}^{M \times N}$  (usually called the measurement matrix) is written as

$$\mathbf{A} = (a_{ij})_{1 \leq i \leq M, 1 \leq j \leq N}, \quad a_{ij} = \psi_j(\mathbf{z}^{(i)}). \quad (3.2)$$

It is well known that this  $\ell_0$  minimization problem (3.1) is NP-hard [84]. As mentioned in Section 2.2, CS is a well-studied and popular approach to find sparse solutions to (3.1) through  $\ell_1$ -minimization shown in (2.6) (no noise) or (2.7) (with noise). Therefore, the approach introduced below can be viewed as a method for data-driven construction of bases that allow sparse representation and accurate recovery for QoIs in UQ applications.

#### 3.1. Data-driven construction of the *amdP* basis

Let us start with a set of samples of  $d$ -dimensional random vector  $\xi \in \mathbb{R}^d$ , i.e.,  $S := \{\xi^{(k)}\}_{k=1}^{N_s}$  with the underlying probability measure  $\rho(\xi)$ .  $S$  is usually called the *sample set*. We aim to construct a set of orthonormal polynomial basis functions  $\{\psi_\alpha(\xi)\}_{|\alpha|=0}^p$  with respect to  $\rho(\xi)$  in  $\Pi_p^d$ , the space of polynomials up to degree  $p$ . Since  $\rho(\xi)$  can be non-Gaussian or even unknown, we do not make the assumption that each component of  $\xi$  is mutually independent, even under a linear transformation such as those based on principal component analysis (PCA). Consequently, the orthogonal polynomial basis  $\psi_\alpha(\xi)$  cannot be directly constructed as a tensor product of univariate orthonormal basis functions in each component of  $\xi$ . Below, we introduce a data-driven approach to construct multivariate *amdP* randomness.

##### 3.1.1. Orthonormal basis

When we have a collection of random samples  $S$ , and the underlying probability measure  $\rho(\xi)$  can be approximated by the discrete measure  $\nu_S(\xi)$

$$\rho(\xi) \approx \nu_S(\xi) := \frac{1}{N_s} \sum_{\xi^{(k)} \in S} \delta_{\xi^{(k)}}(\xi), \quad (3.3)$$

where  $\delta_{\xi^{(k)}}$  is the Dirac measure, that is  $\delta_{\xi^{(k)}}(\xi)$  is equal to 1 when  $\xi = \xi^{(k)}$  and 0 otherwise. Given the inner product defined as in (2.2) with  $\rho$  replaced by the discrete measure  $\nu_S$ , we can construct a set of orthonormal multivariate polynomial basis functions  $\{\psi_\alpha(\xi)\}_{|\alpha|=0}^p$  via the Gram-Schmidt orthogonalization process on  
195 an ordered monomial basis  $\{\hat{\psi}_\alpha(\xi)\}_{|\alpha|=0}^p$ . Here, we use the aforementioned graded lexicographic ordering of the multi-index.

Similar to Dunkl and Xu [76],  $\psi_\alpha$  can be constructed using the recursive formulation

$$\psi_\alpha(\xi) = f_\alpha^\alpha \hat{\psi}_\alpha(\xi) - \sum_{\beta \prec \alpha} f_\beta^\alpha \psi_\beta(\xi), \quad (3.4)$$

where  $\hat{\psi}_\alpha(\xi) := \prod_{k=1}^d \xi_k^{\alpha_k}$  represents the multivariate monomial basis function. The expression  $\beta \prec \alpha$  means that the multi-index  $\beta$  comes before  $\alpha$  under the chosen ordering. The coefficients  $f_\beta^\alpha$  are determined by imposing an orthonormal condition with respect to the discrete measure  $\nu_S$ , i.e.,

$$\begin{aligned} \int \psi_\alpha(\xi) \psi_\beta(\xi) d\rho(\xi) &\approx \int \psi_\alpha(\xi) \psi_\beta(\xi) d\nu_S(\xi) \\ &= \frac{1}{N_s} \sum_{k=1}^{N_s} \psi_\alpha(\xi^{(k)}) \psi_\beta(\xi^{(k)}) \\ &\equiv \delta_{\alpha,\beta}, \quad \beta \preceq \alpha. \end{aligned} \quad (3.5)$$

Equations (3.4) and (3.5) generate a set of orthonormal basis functions on the discrete measure  $\nu_S$  irrespective of the mutual dependence between the components of  $\xi$ . We employ  $\{\psi_\alpha(\xi)\}_{|\alpha|=0}^p$  as the amdP basis on  $\rho(\xi)$ .

Numerically, the modified Gram-Schmidt orthogonalization can be used as an alternative approach when  
200 the number of basis is too large and there exists instability in the standard Gram-Schmidt orthogonalization.

When  $\rho(\xi)$  is known explicitly, orthonormal basis functions can also be constructed by taking the general formulation in Equation (3.4) and imposing the inner product in Equation (2.2) with respect to  $\rho$ . Here we will also consider a special case when  $\xi$  is a random vector that is linearly transformed from a random vector  $z$  with i.i.d. components via  $\xi = Qz$ . This case is motivated by the sparsity enhancement approach discussed  
205 in Sec. 3.2. In particular, we assume that the quadrature rule of polynomial integration with respect to the probability measure of  $z$  is explicitly known.

Given these assumptions,  $f_\beta^\alpha$  can be determined by Equation (3.4) and the orthonormal condition

$$\begin{aligned} \int \psi_\alpha(\xi) \psi_\beta(\xi) d\rho(\xi) &= \sum_{k=1}^{N_Q} \psi_\alpha(Qz_Q^{(k)}) \psi_\beta(Qz_Q^{(k)}) w_k \\ &\equiv \delta_{\alpha,\beta}, \quad \beta \preceq \alpha, \end{aligned} \quad (3.6)$$

where  $\{z_Q^{(k)}\}_{k=1}^{N_Q}$  and  $\{w_k\}_{k=1}^{N_Q}$  represent the quadrature points and weights constructed to yield an exact integration with probability measure of  $z$  for polynomials of degree  $|\alpha| + |\beta|$  or less.

Algorithms 1 and 2 summarize the procedure of orthonormal basis construction when  $\rho(\xi)$  is implicitly  
210 represented by a sample set  $S$  and known explicitly, respectively. There is no unique system of orthogonal

---

ALGORITHM 1: Construct the orthonormal **amdP** basis  $\{\psi_{\alpha}(\xi)\}_{|\alpha|=0}^p$  on discrete sample set  $S$ .

---

- 1: Given sample set  $S = \{\xi^{(k)}\}_{k=1}^{N_s}$ .
  - 2: Given a fixed multi-index order  $\{\alpha^{(l)}\}_{l=1}^N$ .
  - 3: **for**  $l = 1$  to  $N$  **do**
  - 4:   Let  $\alpha = \alpha^{(l)}$ , construct  $\psi_{\alpha}(\xi) = f_{\alpha}^{\alpha} \hat{\psi}_{\alpha}(\xi) - \sum_{\beta \prec \alpha} f_{\beta}^{\alpha} \psi_{\beta}(\xi)$  subject to Equation (3.5).
  - 5: **end for**
- 

ALGORITHM 2: Construct the orthonormal **amdP** basis  $\{\psi_{\alpha}(\xi)\}_{|\alpha|=0}^p$  with probability measure  $\rho(\alpha)$ .

---

- 1: Given a multi-index order  $\{\alpha^{(l)}\}_{l=1}^N$ .
  - 2: **for**  $l = 1$  to  $N$  **do**
  - 3:   Let  $\alpha = \alpha^{(l)}$ , construct  $\psi_{\alpha}(\xi) = f_{\alpha}^{\alpha} \hat{\psi}_{\alpha}(\xi) - \sum_{\beta \prec \alpha} f_{\beta}^{\alpha} \psi_{\beta}(\xi)$  by evaluating the basis inner product using existing quadrature rule or Equation (3.6) if  $\xi$  can be linearly transformed from a random vector with i.i.d. components  $z$  with an explicitly known quadrature rule.
  - 4: **end for**
- 

polynomial basis functions for both scenarios if  $d > 1$ ; different orderings of  $\alpha$  lead to different orthogonal basis [76]. On the other hand, the constructed orthonormal basis is unique up to unitary transformations as we prove in Theorem 3.1.

**Theorem 3.1.** Let  $\{\psi_{\alpha}(\xi)\}_{|\alpha|=0}^p$  be a set of orthonormal polynomial basis with respect to the measure  $\rho(\xi)$ ,  $\xi \in \mathbb{R}^d$ . Denote by  $\Psi(\xi)$  the polynomial basis vector

$$\Psi(\xi) := (\psi_{\alpha^{(1)}}, \dots, \psi_{\alpha^{(N)}})^T, \quad (3.7)$$

where  $\alpha^{(1)}, \dots, \alpha^{(N)}$  is the arrangement of multi-index  $\alpha$  according to a fixed multi-index order. Let  $\chi = Q\xi$ , where  $Q \in \mathbb{R}^{d \times d}$  is invertible. Let  $\{\phi_{\beta}(\chi)\}_{|\beta|=0}^p$  be a set of orthonormal polynomial basis functions with respect to a measure  $\rho'(\chi)$  constructed with order  $\beta^{(1)}, \dots, \beta^{(N)}$ , where  $\rho'(\chi)$  is induced from  $\rho(\xi)$ . Then there exists a unitary matrix  $U$  such that  $\Phi(\chi) = U\Psi(\xi)$ , where  $\Phi(\chi) := (\phi_{\beta^{(1)}}, \dots, \phi_{\beta^{(N)}})^T$  denotes the corresponding polynomial basis vector.

*Proof.* Let  $\hat{\Psi}(\xi)$  be the monomial basis vector. Note that  $\{\psi_{\alpha}(\xi)\}_{|\alpha|=0}^p$  and  $\{\phi_{\beta}(\xi)\}_{|\beta|=0}^p$  are two sets of basis in  $\Pi_p^d$ . There exists transfer matrices  $\mathcal{M}_{\psi}$  and  $\mathcal{M}_{\phi} \in \mathbb{R}^{N \times N}$  such that

$$\Psi(\xi) = \mathcal{M}_{\psi} \hat{\Psi}(\xi), \quad \Phi(\chi) = \mathcal{M}_{\phi} \hat{\Psi}(\xi).$$

With  $\chi = Q\xi$ ,  $\Phi(Q\xi)$  is also a basis in  $\Pi_p^d$ . Then there exists an invertible matrix  $T \in \mathbb{R}^{N \times N}$  such that

$$\Phi(\chi) = \Phi(Q\xi) = T\hat{\Psi}(\xi),$$

which gives  $\Phi(\chi) = \mathcal{U}\Psi(\xi)$ , where  $\mathcal{U} = \mathcal{T}\mathcal{M}_\psi^{-1}$ . Recall  $\{\psi_\alpha(\xi)\}_{|\alpha|=0}^p$  and  $\{\phi_\beta(\chi)\}_{|\beta|=0}^p$  are orthonormal basis with respect to  $\rho(\xi)$  and  $\rho'(\chi)$ , we have

$$\mathbf{I} = \int \Phi(\chi)\Phi(\chi)^T d\rho'(\chi) = \int \mathcal{U}\Psi(\xi)\Psi(\xi)^T \mathcal{U}^T d\rho(\xi) = \mathcal{U}\mathcal{U}^T \quad (3.8)$$

□

We do not need further assumptions on  $\rho(\xi)$  because Theorem 3.1 holds both when  $\rho(\xi)$  is a measure on the continuous random vector  $\xi$  (with probability density function  $\omega(\xi)$ ) or a discrete measure  $\nu_S(\xi)$  on a sample set  $S$ . Furthermore, it is straightforward to show the following Corollary.

**Corollary 1.** Let  $S_1 := \{\xi^{(k)}\}_{k=1}^M$  and  $S_2 := \{\chi^{(k)}\}_{k=1}^M$  be two sets of random sampling points where  $\chi^{(k)} = \mathbf{Q}\xi^{(k)}$  with invertible  $\mathbf{Q}$ . Let  $\mathbf{G}_\xi$  and  $\mathbf{G}_\chi$  be the Gram matrix constructed by  $\Psi(\xi)$  and  $\Phi(\chi)$  defined in Theorem 3.1, i.e.,  $\mathbf{G}_\xi := \sum_{k=1}^M \Psi(\xi^{(k)})\Psi(\xi^{(k)})^T/M$  and  $\mathbf{G}_\chi := \sum_{k=1}^M \Phi(\chi^{(k)})\Phi(\chi^{(k)})^T/M$ . Then  $\mathbf{G}_\cdot$  has invariant  $l_2$  norm, that is,  $\|\mathbf{G}_\xi\|_2 = \|\mathbf{G}_\chi\|_2$ . Moreover,  $\|\mathbf{G}_\xi - \mathbf{I}\|_2 = \|\mathbf{G}_\chi - \mathbf{I}\|_2$ .

In general, the  $l_2$  norm of  $\|\mathbf{G}_\xi - \mathbf{I}\|_2$  is independent of specific monomial order of  $\alpha$  and invariant under linear transformations of the random vector. The basis functions  $\{\psi_\alpha(\xi)\}_{|\alpha|=0}^p$  constructed by Equations (3.4) and (3.5) provide an appropriate candidate for representing the surrogate model  $f(\xi)$  via CS.

### 3.1.2. Near-orthonormal basis

When  $\rho(\xi)$  is implicitly represented by a sample set  $S$ , we employ the discrete measure  $\nu_S$  to construct  $\{\psi_\alpha(\xi)\}_{|\beta|=0}^p$ . However, we note that the training set that queries  $f(\cdot)$ , denoted by  $S_f$ , may not be a subset of  $S$ . In practice, the sample set  $S$  and the training set  $S_f$  are usually collected in a sequential manner or directly from different experiments, although individual sampling points of both  $S$  and  $S_f$  follow the same distribution. Since  $S$  only contains a finite number of samples of  $\xi$ , basis  $\{\psi_\alpha(\xi)\}_{|\alpha|=0}^p$  constructed by (3.4) and (3.5) is not the “exact orthonormal” basis with respect to  $\rho(\xi)$ . Especially, let  $S' = \{\xi'_k\}_{k=1}^{N_s}$  be another sample set following the same distribution  $\rho(\cdot)$  and  $\nu_{S'}(\cdot)$  be the discrete measure defined on  $S'$ . For the orthonormal **amdP** basis functions  $\{\psi_\alpha(\xi)\}_{|\alpha|=0}^p$  constructed on  $S$ , we have  $\mathbb{E}[\Psi(\xi)\Psi(\xi)^T] \neq \mathbf{I}$  under the discrete measure  $\nu_{S'}(\xi)$  and vice versa.

The above observation forces us to re-examine the orthonormal condition imposed by (3.5). Since the pre-constructed basis  $\psi_\alpha(\xi)$  does not retain the exact orthonormal condition when later being applied to approximate  $f(\xi)$ , we may relax the condition when determining the coefficients  $f_\beta^\alpha$  in (3.4). In the present study, we propose the following heuristic criterion

$$\arg \min_{\hat{\mathbf{f}}^\alpha} \|\hat{\mathbf{f}}^\alpha\|_2 \text{ subject to } \left| \int \psi_\alpha(\xi)\psi_\beta(\xi) d\nu_S(\xi) - \delta_{\alpha,\beta} \right| < \zeta_{\alpha,\beta}, \quad \beta \leq \alpha, \quad (3.9)$$

where  $\hat{\mathbf{f}}^\alpha$  is the coefficient vector of  $\psi_\alpha$  when represented using monomial basis functions, i.e.,  $\psi_\alpha(\xi) = \sum_{\beta \leq \alpha} \hat{f}_\beta^\alpha \hat{\psi}_\beta(\xi)$ .  $\hat{\mathbf{f}}^\alpha$  is related to  $\mathbf{f}^\alpha$  through the linear transformation

$$\hat{\mathbf{f}}^\alpha = \begin{pmatrix} \mathbf{F} & 0 \\ 0 & 1 \end{pmatrix} \mathbf{f}^\alpha, \quad (3.10)$$

where  $\mathbf{F}$  is an upper triangle matrix determined by pre-computed  $\hat{\mathbf{f}}^\beta, \beta \prec \alpha$ , i.e.,

$$[\mathbf{F}]_{I_{\beta'} I_\beta} = \begin{cases} \hat{f}_{\beta'}^\beta & \beta' \preceq \beta \\ 0 & \beta' \succ \beta, \end{cases} \quad (3.11)$$

<sup>240</sup> where  $I_\beta$  represents the mapping from multi-index to single index.

The parameter  $\zeta_{\alpha, \beta}$  quantifies the relaxation of the orthonormal condition. We split the sample set  $S$  equally into two parts  $S := S_1 \cup S_2$ . Denote  $\{\psi_\alpha^{(1)}(\xi)\}_{|\alpha|=0}^p$  and  $\{\psi_\alpha^{(2)}(\xi)\}_{|\alpha|=0}^p$  the orthonormal bases constructed by Equations (3.4) and (3.5) on the discrete measures  $\nu_{S_1}(\xi)$  and  $\nu_{S_2}(\xi)$ , respectively. Inspired by cross-validation, we have chosen  $\zeta_{\alpha, \beta} = \frac{|\zeta_1| + |\zeta_2|}{2\sqrt{2}}$

$$\zeta_1 = \int \psi_\alpha^{(1)}(\xi) \psi_\beta^{(1)}(\xi) d\nu_{S_2}(\xi), \quad \zeta_2 = \int \psi_\alpha^{(2)}(\xi) \psi_\beta^{(2)}(\xi) d\nu_{S_1}(\xi). \quad (3.12)$$

ALGORITHM 3: Construct the near-orthonormal **amdP** basis  $\{\psi_\alpha(\xi)\}_{|\alpha|=0}^p$  on discrete sample set  $S$ .

- 1: Collect samples of  $\xi$  from sample set  $S = \{\xi^{(k)}\}_{k=1}^{N_s}$ , split  $S$  equally into two disjoint subsets, i.e.,  $S = S_1 \cup S_2$ ,  $S_1 \cap S_2 = \emptyset$ .
- 2: Given fixed monomial index order  $\{\alpha^{(l)}\}_{l=1}^N$ , construct the orthonormal **amdP** basis  $\{\psi_\alpha^{(1)}(\xi)\}_{|\alpha|=0}^p$  and  $\{\psi_\alpha^{(2)}(\xi)\}_{|\alpha|=0}^p$  on set  $S_1$  and  $S_2$  by **Algorithm 1**.
- 3: **for**  $l = 1$  to  $N$  **do**
- 4:   Let  $\alpha = \alpha^{(l)}$ , construct  $\psi_\alpha(\xi) = f_\alpha^\alpha \hat{\psi}_\alpha(\xi) - \sum_{\beta \prec \alpha} f_\beta^\alpha \psi_\beta(\xi)$  on by Equations (3.9), (3.10), and (3.12).
- 5: **end for**

Algorithm 3 describes construction for a set of near-orthonormal **amdP** basis functions on the sample set  $S$ . When applied to the sample set  $S'$  to approximate  $f(\xi)$ , the basis shows comparable orthonormal conditions with the basis constructed by (3.5). Such results can be partially understood by the theoretical bound from Theorem 2.5 on the number of samples  $M$  for exact recovery in orthonormal polynomial systems,  
<sup>245</sup>  $M \geq C_1 K^2 s \log^3(s) \log(N)$ , where  $s = \|c\|_0$  and  $K = \sup_\alpha \|\psi_\alpha\|_\infty$ . Theoretical analysis of the recovery error under different basis functions is out of the scope of the present work and is left for future investigation. However, we note that the accuracy of the surrogate model  $f(\xi)$  can be further improved by enhancing

the sparsity of  $\mathbf{c}$ . This can be achieved through the ideas presented in our previous work [1] which will be extended to general distributions below.

**Remark 3.2.** We emphasize that (3.9) provides a heuristic approach to construct the near-orthonormal **amdP** basis functions  $\psi_\alpha(\xi)$  with a smaller basis bound. In practice, (3.9) can be further relaxed to

$$\begin{aligned} \arg \min_{\hat{\mathbf{f}}^\alpha} \|\hat{\mathbf{f}}^\alpha\|_2 \text{ subject to } & \sum_{|\beta|=r, \beta < \alpha} \left| \int \psi_\alpha(\xi) \psi_\beta(\xi) d\nu_S(\xi) \right|^2 < \sum_{|\beta|=r, \beta < \alpha} \zeta_{\alpha,\beta}^2, \\ & \left| \int \psi_\alpha(\xi) \psi_\alpha(\xi) d\nu_S(\xi) - 1 \right| < \zeta_{\alpha,\alpha}, \quad r = 0, \dots, |\alpha|, \end{aligned} \quad (3.13)$$

which shows similar numerical performance. There is no theoretical guarantee yet that Equations (3.9) and (3.13) yield a smaller basis bound than (3.5) on  $S_f$ ,  $S$  or the entire domain of  $\xi$ . We numerically compare some properties of different bases in Section 4.1, which illustrate the performance of the near-orthonormal **amdP** basis constructed above. There may exist other numerical approaches to optimize  $\psi_\alpha(\xi)$  that can lead to an even smaller basis bound. We also note that the threshold  $\zeta_{\alpha,\beta}$  is determined by directly splitting  $S$  into two disjoint sets. In practice, it is possible to design more sophisticated strategies to optimize the choice of  $\zeta_{\alpha,\beta}$  and the basis construction procedure. We leave such studies for future work.

### 3.2. Sparsity enhancement

For the linear system in (2.6), the numerical accuracy of the recovered  $\tilde{\mathbf{c}}$  via  $l_1$ -minimization depends on the sparsity of  $\mathbf{c}$ . This dependence motivates us to develop a numerical approach to further enhance the sparsity of  $\mathbf{c}$  through the variability analysis of  $f(\xi)$  [1]. If we know  $f(\xi)$  explicitly, the (sorted) directions of variance in  $f(\xi)$  under the distribution of  $\xi$  can be found based on the active subspace method [85, 66]. In particular, we define the gradient matrix  $\mathbf{G}$  by

$$\mathbf{G} = \mathbb{E} \left[ \nabla f(\xi) \nabla f(\xi)^T \right] \quad (3.14)$$

where  $\nabla f(\xi)$  is the gradient vector defined by  $\nabla f(\xi) = \left( \frac{\partial f}{\partial \xi_1}, \frac{\partial f}{\partial \xi_2}, \dots, \frac{\partial f}{\partial \xi_d} \right)^T$ . Eigendecomposition of  $\mathbf{G}$ ,

$$\mathbf{G} = \mathbf{Q} \mathbf{K} \mathbf{Q}^T, \quad \mathbf{Q} = [\mathbf{q}_1 \ \mathbf{q}_2 \ \dots \ \mathbf{q}_d], \quad (3.15a)$$

$$\mathbf{K} = \text{diag}(k_1, \dots, k_d), \quad k_1 \geq \dots \geq k_d \geq 0, \quad (3.15b)$$

yields the sorted variability directions  $\mathbf{q}_1, \mathbf{q}_2, \dots, \mathbf{q}_d$ . Accordingly, we may define a new random vector  $\chi$  following the sorted variability directions via linear transformation

$$\chi = \mathbf{Q}^T \xi. \quad (3.16)$$

$f(\xi) = f((\mathbf{Q}^T)^{-1} \chi) = f(\mathbf{Q} \chi)$  can be approximated by expansion in an orthonormal polynomial basis  $\chi$  with a coefficient vector  $\mathbf{c}$  which is sparser than the  $f(\xi)$  being expanded by orthonormal basis of  $\xi$ . For the

260 remainder of this paper, we use  $\mathbf{Q}$  to denote the rotation matrix to transform  $\xi$  to  $\chi$  and  $g(\chi)$  to represent  $f(\mathbf{Q}\chi)$ .

In practice,  $f(\xi)$  is usually not explicitly known. We may numerically approximate  $\mathbf{G}$  by

$$\mathbf{G} \approx \mathbb{E} \left[ \nabla \tilde{f}(\xi) \nabla \tilde{f}(\xi)^T \right], \quad (3.17)$$

where  $\tilde{f}(\xi)$  represents the approximation of  $f(\xi)$  by the orthonormal polynomial basis functions  $\psi_\alpha(\xi)$  as proposed in [1] or obtained via solving (2.6) with the data-driven basis approach (i.e., basis functions constructed with respect to an arbitrary measure) described in Section 3.1. In particular, if  $\xi$  is a random  
265 vector with i.i.d. Gaussian components,  $\chi$  is also a random vector with i.i.d. Gaussian components. Thus,  $\tilde{f}(\xi)$  and  $\tilde{g}(\chi) := \tilde{f}(\mathbf{Q}\chi)$  can be represented by the orthonormal basis functions of the same form, e.g., tensor products of univariate Hermite polynomials. Without loss of generality, from now on, we use  $\tilde{g}(\chi)$  to represent  $\tilde{f}(\mathbf{Q}\chi)$ .

However, if  $\rho(\xi)$  is not i.i.d. Gaussian,  $\chi$  and  $\xi$  do not generally have the same distribution. Therefore,  
270 an orthonormal polynomial basis  $\psi(\cdot)$  with respect to  $\xi$  cannot be directly applied to  $\chi$ . The general approach presented in Section 3.1 enables us to construct the **amdP** basis with respect to the probability measure of the rotated vector  $\chi$ . The two orthonormal bases associated with  $\xi$  and  $\chi$  respectively are related to each other via a unitary transformation as shown in Theorem 3.1. In particular, if  $\rho(\xi)$  is implicitly described by a sample set  $S = \{\xi^{(k)}\}_{k=1}^{N_s}$ ,  $\mathbf{G}$  can be easily evaluated by representing  $\psi_\alpha(\xi)$  via the monomial basis, i.e.,  
275  $\psi_\alpha(\xi) = \sum_{\beta \leq \alpha} \hat{f}_\beta^\alpha \hat{\psi}_\beta(\xi)$  via Equation (3.10) and then integrating with discrete measure  $\nu_S$ . By transforming  $S$  and  $S_f$  into  $\{\chi^{(k)}\}_{k=1}^{N_s}$  and  $\{\chi'^{(k)}\}_{k=1}^M$ , the orthonormal and near-orthonormal **amdP** basis functions with respect to  $\chi$  can be constructed by Eqs. (3.5) (3.13). The surrogate model  $\tilde{g}(\chi)$  can then be constructed by solving (2.6).

The entire DSRAR procedure is presented in **Algorithm 4**. Compared with  $\tilde{f}(\xi)$ ,  $\tilde{g}(\chi)$  shows smaller  
280 numerical error in general. The additional cost of sparsity enhancement procedure in Step 4 - 6 is less than 0.6 CPU (3.7 GHz Quad-Core Intel Xeon E5) hour for the numerical examples considered in this study. For realistic applications, the overhead of Step 4 - 6 could be relatively small if sampling of QoI is expensive or the available training set is limited.

The DSRAR framework described above is also applicable to systems with standard density distributions,  
285 where  $\rho(\xi)$  is known explicitly. Without loss of generality, we assume that an orthonormal polynomial basis  $\{\psi_\alpha(\xi)\}_{|\alpha|=0}^p$  is known. Evaluation of  $\mathbf{G}$  by (3.17) on  $\rho(\xi)$  is straightforward. The surrogate model of  $f$  can be constructed via  $l_1$  minimization with enhanced sparsity through Algorithm 5.

The procedures for random vector rotation and surrogate construction presented in Algorithms 4 and 5 can be conducted in an iterative manner. We have investigated this issue [86] by applying a previously  
290 developed rotation procedure [1] successively to systems with underlying Gaussian distributions. For the

---

ALGORITHM 4: DSRAR: Surrogate model construction with discrete sample set  $S$  and training set  $S_f$ .

---

- 1: Collect the sample set within the random space  $S = \{\xi^{(k)}\}_{k=1}^{N_s}$ .
  - 2: Generate evaluations of  $f$  on training set  $S_f = \{\xi'^{(k)}\}_{k=1}^M$  with  $M$  outputs  $f_1, f_2, \dots, f_M$ .
  - 3: Construct the data-driven **amdP** basis  $\{\psi_i(\xi)\}_{i=1}^N$  on discrete measure  $\nu_S(\xi)$  as the exact orthonormal basis by Algorithm 1 or the near orthonormal basis by Algorithm 3.
  - 4: Evaluate the measurement matrix  $A_{ij} = \psi_j(\xi'^{(i)})$ ,  $1 \leq i \leq M$ ,  $1 \leq j \leq N$ ; construct surrogate model  $\tilde{f}(\xi) = \sum_{|\alpha|=0}^p c_\alpha \psi_\alpha(\xi)$  by solving the  $l_1$ -minimization problem.
  - 5: Evaluate the gradient matrix  $\mathbf{G} \approx \mathbb{E} [\nabla \tilde{f}(\xi) \nabla \tilde{f}(\xi)^T]$  on  $\nu_S(\xi)$ . Find the eigendecomposition  $\mathbf{G} = \mathbf{Q} \mathbf{K} \mathbf{Q}^T$ , define sample set  $\{\chi^{(k)}\}_{k=1}^{N_s}$  and training set  $\{\chi'^{(k)}\}_{k=1}^M$  by  $\chi^{(k)} = \mathbf{Q}^T \xi^{(k)}$ ,  $\chi'^{(k)} = \mathbf{Q}^T \xi'^{(k)}$ .
  - 6: Reconstruct the data-driven **amdP** basis  $\{\phi_\alpha(\chi)\}_{|\alpha|=0}^p$  by Algorithm 3 and surrogate model  $\tilde{g}(\chi)$  with enhanced sparsity following Step 3 and Step 4.
- 

---

ALGORITHM 5: DSRAR: Surrogate model construction with training set  $S_f$  and probability measure  $\rho(\xi)$ .

---

- 1: Evaluate  $f$  on training set  $S_f = \{\xi'^{(k)}\}_{k=1}^M$  with  $M$  outputs  $f_1, f_2, \dots, f_M$ .
  - 2: Evaluate the measurement matrix  $A_{ij} = \psi_j(\xi'^{(i)})$ ,  $1 \leq i \leq M$ ,  $1 \leq j \leq N$ ; construct surrogate model  $\tilde{f}(\xi) = \sum_{|\alpha|=0}^p c_\alpha \psi_\alpha(\xi)$  by solving  $l_1$  minimization problem.
  - 3: Evaluate the gradient matrix  $\mathbf{G} = \mathbb{E} [\nabla \tilde{f}(\xi) \nabla \tilde{f}(\xi)^T]$  on  $\rho(\xi)$ . Conduct eigendecomposition  $\mathbf{G} = \mathbf{Q} \mathbf{K} \mathbf{Q}^T$  and define training set  $\{\chi'^{(k)}\}_{k=1}^M$ ,  $\chi'^{(k)} = \mathbf{Q}^T \xi'^{(k)}$ .
  - 4: Re-construct the orthonormal **amdP** basis  $\{\phi_\alpha(\chi)\}_{|\alpha|=0}^p$  with respect to  $\rho'(\chi)$  by **Algorithm 2**. Construct the surrogate model  $\tilde{g}(\chi)$  with enhanced sparsity following Step 3.
-

systems studied in the present work, the improvement of the numerical accuracy is marginal after the first rotation procedure. Therefore, the numerical results with only one rotation procedure will be presented in this manuscript.

## 4. Results

This section presents the numerical results of the present DSRAR framework for surrogate model construction with arbitrary underlying distributions. For numerical examples where the probability measure  $\rho(\xi)$  (with density function  $\omega(\xi)$ ) is not known explicitly and is represented by a discrete data set  $S = \{\xi^{(k)}\}_{k=1}^{N_s}$ , we split  $S$  equally into two subsets  $S = S_1 \cup S_2$ . We use  $S_1$  to construct the data-driven **amdP** basis and split  $S_2$  into two disjoint subset  $S_2 = S_{2,1} \cup S_{2,2}$ , where  $S_{2,1}$  is the training set for surrogate model construction and  $S_{2,2}$  is the test set to evaluate the accuracy of the constructed surrogate model. The size of the training set is  $O(10^2) - O(10^3)$  and size of the test set is  $O(10^5)$ .

### 4.1. Accurate recovery of linear systems with data-driven bases

In this test, we collected a sample set  $S = \{\xi^{(k)}\}_{k=1}^{N_s}$  with  $N_s = 2 \times 10^5$ . The random vector  $\xi$  followed the Gaussian mixture distribution

$$\omega(\xi) = \sum_{i=1}^{N_m} a_i \mathcal{N}(\mu_i, \Sigma_i) \quad (4.1)$$

where  $N_m$  is the number of Gaussian modes. We set  $N_m = 3$ ,  $a_i > 0$  for  $i = 1, 2, 3$  and  $\sum_{i=1}^3 a_i = 1$ . For each Gaussian mode,  $\mu_i$  is a 25-dimensional i.i.d. random vector with uniform distribution  $\mathcal{U}[-2.5, 2.5]$  on each dimension and then shifted such that  $\sum_{i=1}^3 a_i \mu_i = 0$ . The matrices  $\Sigma_i$  were chosen such that

$$\Sigma_i = (\Upsilon_i \Upsilon_i^T + \mathbf{I})/4, \quad (4.2)$$

where  $\Upsilon_i$  is a random matrix with i.i.d. entries from  $\mathcal{U}[0, 1]$  for  $i = 1, 2, 3$ .

We considered a linear system

$$A\mathbf{c} = \mathbf{b} + \boldsymbol{\varepsilon}$$

and recovered  $\mathbf{c}$  using  $M$  training points by solving the  $l_1$  minimization problem defined by (2.6) where

$$[A]_{i,j} = \psi_j(\xi^{(i)}), \quad b_i = \sum_{k=1}^N c_k \psi_k(\xi^{(i)}), \quad (4.3)$$

with  $1 \leq i \leq M$ ,  $1 \leq j \leq N$ , and  $\boldsymbol{\varepsilon}$  is noise with  $\|\boldsymbol{\varepsilon}\|_2 \leq 10^{-7}$ . We set  $d = 25$ ,  $p = 2$  and  $N = \begin{pmatrix} d+p \\ p \end{pmatrix} = 351$ . The basis functions  $\psi_\alpha(\xi)$  were constructed on the set  $S_1$  by the following approaches:

1. the orthonormal **amdP** basis subject to Equations (3.4) and (3.5);
2. the near-orthonormal **amdP** basis subject to Equation (3.9);

3. tensor product of univariate normalized Legendre polynomials (both sampling points and training points are scaled to lie in  $[-1, 1]$  on each dimension accordingly).
- 310 Training points from set  $S_2$  were used to examine the recovery accuracy of  $\mathbf{c}$ .

#### 4.1.1. Sparse linear systems

First, we considered the scenario where  $\mathbf{c}$  is a  $s$ -sparse vector and employed the following theoretical bound to examine the recovery accuracy via  $\ell_1$ -minimization.

**Theorem 4.1.** *Given a matrix  $\Psi \in \mathbb{R}^{M \times N}$  and set  $T_\alpha$  with  $s = |T_\alpha|$ , a  $s$ -sparse vector  $\mathbf{c}$  with non-zero entries on  $T_\alpha$  can be exactly recovered via  $\ell_1$ -minimization if  $\frac{\theta_s}{1-\delta_s} < 0.5$ , where  $\delta_s$  and  $\theta_s$  are defined by*

$$\begin{aligned}\delta_s &:= \inf [\delta : (1-\delta)\|\mathbf{y}\|_2^2 \leq \|\Psi_t \mathbf{y}\|_2^2 \leq (1+\delta)\|\mathbf{y}\|_2^2], \quad \forall t \subseteq \mathbf{T}, \forall \mathbf{y} \in \mathbb{R}^{|t|} \\ \theta_s &:= \inf [\theta : |\langle \Psi_{t'}, \Psi_t \mathbf{y}' \rangle| \leq \theta \|\mathbf{y}'\|_2 \|\mathbf{y}\|_2], \quad \forall t \subseteq \mathbf{T}, t' \not\subseteq \mathbf{T}, |t'| \leq s, \forall \mathbf{y} \in \mathbb{R}^{|t|}, \mathbf{y}' \in \mathbb{R}^{|t'|}\end{aligned}\tag{4.4}$$

where  $\Psi_t$  and  $\Psi_{t'}$  denote the sub-matrices of  $\Psi$  with column indices in  $t$  and  $t'$  respectively.

- 315 Theorem 4.1 (see Appendix A for proof) provides a sufficient condition to exactly recover  $\mathbf{c}$  with non-zero entries on index set  $T_\alpha$ . For numerical study, we randomly chose an index set  $T_\alpha$  from  $\Lambda_p^d$  with  $|T_\alpha| = 3$ , where  $\Lambda_p^d$  is defined by (2.4). For each training set, we constructed the measurement matrix  $\mathbf{A}$  with different bases and computed  $\theta_s / (1 - \delta_s)$  by (4.4). Figure 1(a) shows the mean value  $\mathbb{E}[\theta_s / (1 - \delta_s)]$  on 200 independent training sets chosen from  $S_2$  for each  $M$ . The exact and near-orthonormal bases yield 320 similar results:  $\mathbb{E}[\theta_s / (1 - \delta_s)]$  becomes smaller than 0.5 as  $M$  approaches 210, which is also shown in the inset plot of Figure 1(a). In contrast,  $\mathbb{E}[\theta_s / (1 - \delta_s)]$  obtained from Legendre polynomial basis shows worse performance due to the loss of orthonormality.

- In our numerical experiments, we were able to recover  $\mathbf{c}$  using fewer samples than the number  $M$ —as 325 suggested by the sufficient condition (Theorem 2.5) originally given by Rauhut [52]—since this number is based on the worst case scenario and is not, in general, a sharp bound. Figure 1(b) shows the numerical results of a test case with  $c_{T_\alpha} = 1$ ,  $c_{T_\alpha^c} = 0$ ,  $|T_\alpha| = 5$ . For each  $M$ , 200 CS implementations were conducted to compute the average of the relative error  $\|\mathbf{c} - \tilde{\mathbf{c}}\|_1 / \|\mathbf{c}\|_1$ . The exact and near-orthonormal `amdP` bases show similar performance, where  $\mathbf{c}$  can be accurately recovered (up to  $\|\varepsilon\|_2$ ) using  $M = 45$  training points. In contrast, the Legendre basis yields larger relative error in  $\ell_1$ -norm. The relative error of the recovered 330 coefficients from one CS implementation with Legendre basis is shown in the inset plot of Figure 1(b).

#### 4.1.2. Non-sparse linear systems

We also tested the recovery performance when the exact representation is not sparse. The vector  $\mathbf{c}$  is chosen with a random non-zero index set  $T_\alpha$  with  $|T_\alpha| = 120$ . Individual components of  $\mathbf{c}_{T_\alpha}$  are i.i.d. log-normal, such that  $\log \mathbf{c}_{T_\alpha} \sim \mathcal{N}(0, 2)$ . For each size ( $M$ ) of the training set, 200 CS implementations were

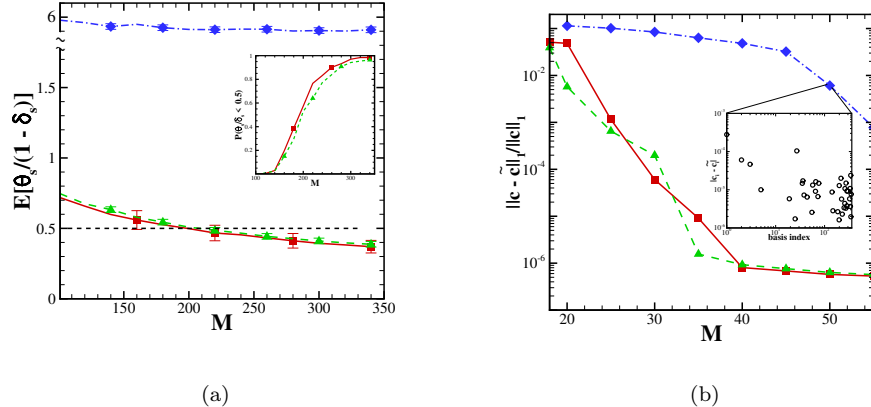


Figure 1: The measurement matrices constructed by the exact and near-orthonormal bases exhibit similar performance in the theoretical (sufficient) bound and numerical results for recovery of sparse vector. Both bases outperform the Legendre basis.  
 “”: the exact orthonormal `amdP` basis; “”: the near-orthonormal `amdP` basis; “”: Legendre basis.  
 (a) Mean value of the theoretical bound  $\mathbb{E}[\theta_s / (1 - \delta_s)]$  of exact recovery for measurement matrices  $\mathbf{A}$  constructed by various bases for the chosen non-zero index  $T_\alpha$  with  $s = 3$ . The error bar represents the standard deviation. The inset plot shows the theoretical prediction of the exact recovery probability. (b) Relative  $l_1$  error of the recovered sparse vector ( $s = 5$ ) using different training set size  $M$ . The inset plot shows the recovery error  $\|\mathbf{c} - \tilde{\mathbf{c}}\|_1$  of one training set for the Legendre basis system.

335 conducted to compute the average of the numerical error  $\|\mathbf{c} - \tilde{\mathbf{c}}\|_2$ , as shown in Figure 2(a). Similar to the previous example, the Legendre basis exhibits the largest approximation error. The near-orthonormal basis shows smaller error than the exact orthonormal basis.

We also computed the density distribution of individual component  $|c_{i'} - \tilde{c}_{i'}|$ , where  $i'$  refers to single index sorted by the magnitude in descending order. Figure 2(b-d) shows that, compared with the exact orthonormal basis and the Legendre basis, the distribution of  $\log |c_{i'} - \tilde{c}_{i'}|$  obtained from near-orthonormal basis is biased toward the smallest magnitudes for error of individual  $i'$ . This result can be interpreted as that the average of  $\|\mathbf{c} - \tilde{\mathbf{c}}\|_2$  of the near orthogonal basis is smaller than that of the exact orthogonal basis and also outperforms the Legendre basis.

#### 4.2. Systems with explicit knowledge of density function

345 In this subsection, we demonstrate the proposed method in systems with common non-Gaussian randomness with analytical density function  $\omega(\xi)$ . We show that the present method based on orthonormal basis construction and rotation of the random variables exploits the sparser representation of QoI while retaining proper orthogonality with respect to rotated variables. Therefore, it yields more accurate surrogate models than other approaches based on the direct recovery of  $c$  without the sparsity enhancement rotation procedure  
 350 and/or directly applying the rotation procedure without reconstruction of the orthonormal **amdP** basis.

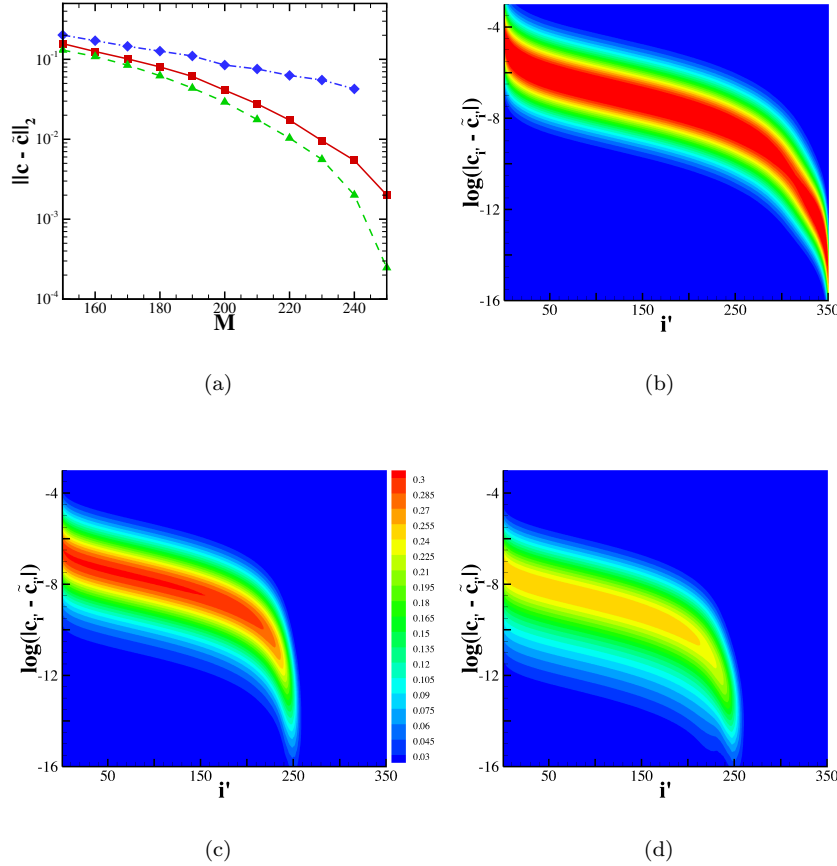


Figure 2: The measurement matrices constructed by different bases show different numerical performance for the recovery of non-sparse vector. The near-orthonormal basis shows the most accurate result. (a)  $l_1$  error of the recovered vector  $\mathbf{c}$  with different bases. “ $\textcolor{red}{—■—}$ ”: the exact orthonormal `amdP` basis; “ $\textcolor{green}{-▲-}$ ”: the near-orthonormal `amdP` basis; “ $\textcolor{blue}{-◆-}$ ”: Legendre basis. (b-d) Contours of  $|\mathbf{c}_{\alpha'} - \tilde{\mathbf{c}}_{\alpha'}|$  (sorted by magnitude) from training sets of size  $M = 230$  with Legendre (top right), orthonormal (bottom left) and near-orthonormal bases (bottom right).

#### 4.2.1. High-dimensional polynomial

For the first numerical example, we consider a high-dimensional polynomial function

$$f(\xi) = \sum_{|\alpha| \leq 3} \hat{c}_\alpha \hat{\psi}_\alpha(\xi) = \sum_{i=1}^N \frac{\eta_i}{|i|^{1.5}} \hat{\psi}_i(\xi), \quad (4.5)$$

where  $\hat{\psi}_\alpha$  and  $\hat{\psi}_i$  represent monomial basis functions,  $\eta_i$  represents uniform random variables  $\mathcal{U}[0, 1]$ . We employed this polynomial function with sparse coefficients as a benchmark problem to examine the recovery accuracy of the present method.  $\xi$  is a random vector consisting of 20 i.i.d. random variables. The density function of the  $i$ -th variable  $\xi_i$  is given by

$$\omega(\xi_i) = e^{-\xi_i}, \quad (4.6)$$

where the corresponding orthonormal basis are given by the Laguerre polynomials. Accordingly, we construct a 3<sup>rd</sup>-order polynomial expansion  $\tilde{f}(\xi)$  with  $N = 1771$  multivariate basis functions, which are the tensor product of the univariate Laguerre polynomials. Figure 3 shows the relative  $l_2$  error of  $\tilde{f}$  computed by level 355 4 sparse grid integration. Similar to the previous example, the probability density function (PDF) of  $\chi$  does not retain the form  $\omega'(\chi) = \prod_{i=1}^d \exp(-\chi_i)$  after the rotation. Iteratively employing the multivariate Laguerre polynomials to represent  $\tilde{g}(\chi)$  may result in erroneous prediction (the red dash-dotted curve). Alternatively, such a problem can be addressed by using the reconstructed orthonormal **amdP** basis with respect to  $\chi$ , which yields a smaller error than  $\tilde{f}(\xi)$  (the blue dashed curve).

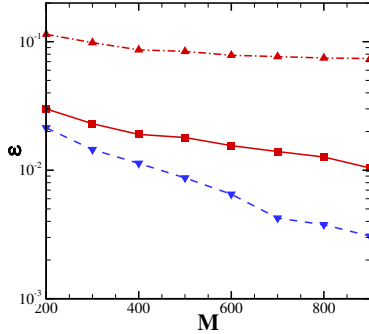


Figure 3: Sparsity-enhancing rotation with the reconstructed orthonormal **amdP** basis yields the most accurate recovery of a high-dimensional polynomial function of random vectors following density function given by Equation (4.6). Directly applying the rotation procedure without reconstructing the orthonormal basis yields erroneous prediction. “—■—”: Laguerre polynomial basis with respect to  $\xi$ ; “---▲---”: Laguerre polynomial basis with respect to rotated vector  $\chi$ ; “---▼---”: the reconstructed **amdP** orthonormal basis with respect to rotated vector  $\chi$ .

We applied the proposed method to model the solution to a one-dimensional (1D) elliptic PDE with high dimensional random input

$$\begin{aligned} -\frac{d}{dx} \left( D(x; \boldsymbol{\xi}) \frac{du(x; \boldsymbol{\xi})}{dx} \right) &= 1, \quad x \in (0, 1) \\ u(0) = u(1) &= 0, \end{aligned} \tag{4.7}$$

where  $a(x; \boldsymbol{\xi}) := \log D(x; \boldsymbol{\xi})$  is the stochastic input and  $a(x; \boldsymbol{\xi})$  was a stationary process with correlation function

$$K(x, x') = \exp \left( \frac{|x - x'|}{l_c} \right), \tag{4.8}$$

where  $l_c$  is the correlation length. We constructed  $a(x; \boldsymbol{\xi})$  by the Karhunen-Loève (KL) expansion:

$$a(x; \boldsymbol{\xi}) = a_0(x) + \sigma \sum_{i=1}^d \sqrt{\lambda_i} \phi_i(x) \xi_i, \tag{4.9}$$

where  $\{\lambda_i\}_{i=1}^d$ , and  $\{\phi_i(x)\}_{i=1}^d$  are the  $d$  largest eigenvalues and the corresponding eigenfunctions of  $K(x, x')$ . The values of  $\lambda_i$  and the analytical expressions for  $\phi_i$  were available from the literature [87]. The  $\xi_i$  are i.i.d. random variables on  $[-1, 1]$ . The density function of  $\xi_i$  is given by

$$\omega(\xi_i) = \frac{1}{\pi \sqrt{1 - \xi_i^2}}, \tag{4.10}$$

where the corresponding orthonormal basis consists of Chebyshev polynomials of the first kind. For this example, we set  $a_0(x) \equiv 1$ ,  $\sigma = 0.8$ ,  $l_c = 0.14$  and  $d = 16$ . We chose the quantity of interest as  $u(x; \boldsymbol{\xi})$  at  $x = 0.45$  and constructed a 3<sup>rd</sup>-order polynomial expansion with  $N = 969$  basis functions. Figure 4 shows the relative  $l_2$  error of the constructed  $\tilde{f}(\boldsymbol{\xi})$  and  $\tilde{g}(\boldsymbol{\chi})$ . For the density function  $\omega(\xi_i)$  given by (4.10),  $\tilde{f}(\boldsymbol{\xi})$  can be represented by a multivariate basis constructed by the tensor products of univariate Chebyshev polynomials. However, in general, the PDF of  $\boldsymbol{\chi}$  does not retain the form  $\omega'(\boldsymbol{\chi}) = \prod_{i=1}^d \frac{1}{\pi \sqrt{1 - \chi_i^2}}$ . As shown in Figure 4, iteratively employing the multivariate Chebyshev polynomials to represent  $\tilde{g}(\boldsymbol{\chi})$  (the red dash-dotted curve)—as done in previous studies [88]—resulted in a larger error than  $\tilde{f}(\boldsymbol{\xi})$ . Representing  $\tilde{g}(\boldsymbol{\chi})$  by the reconstructed orthonormal **amdP** basis (the blue dashed curve) further decreases the numerical error compared to  $\tilde{f}(\boldsymbol{\xi})$  (the solid red curve).

### 4.3. Systems with implicit knowledge of density function

In this suite of benchmark examples, we investigated the applicability and efficiency of the developed DSRAR framework based on data-driven orthonormal bases construction and sparsity enhanced rotation.

#### 4.3.1. High-dimensional polynomials

We studied the ability of the data-driven method to recover a high-dimensional polynomial function

$$f(\boldsymbol{\xi}) = \sum_{\alpha \in T_\alpha} \hat{\psi}_\alpha(\boldsymbol{\xi}), \tag{4.11}$$

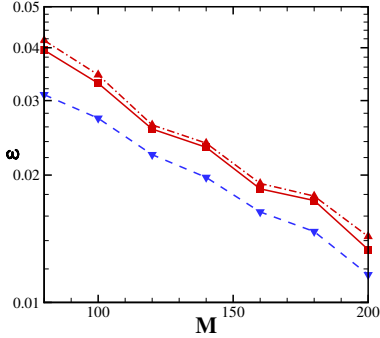


Figure 4: Sparsity-enhancing rotation with reconstructed orthonormal basis yield the most accurate surrogate models for a 1D elliptical PDE with random permeability coefficient modeled by Equations (4.9) and (4.10). Directly applying the rotation procedure without reconstructing the orthonormal basis yields increased numerical error. “ $\text{---} \blacksquare \text{---}$ ”: Chebyshev polynomial basis with respect to  $\xi$ ; “ $\text{---} \blacktriangle \text{---}$ ”: Chebyshev polynomial basis with respect to rotated vector  $\chi$ ; “ $\text{---} \blacktriangledown \text{---}$ ”: the reconstructed orthonormal `amdP` basis with respect to rotated vector  $\chi$ .

375 where  $\hat{\psi}_\alpha$  represents the monomial basis function,  $T_\alpha$  represents a set containing 50 indices randomly chosen from  $\Lambda_p^d$  with  $d = 25$  and  $p = 3$ . The sample set  $S$  of random vector  $\xi$  for basis construction was generated from the Gaussian mixture model specified in (4.1) with  $|S| = 2 \times 10^5$ .

We approximated  $f(\xi)$  by a 3<sup>rd</sup>-order polynomial expansion  $\tilde{f}(\xi) = \sum_{i=1}^N \tilde{c}_i \psi_i(\xi)$  with  $N = 3276$ . Figure 5(a) shows the relative  $l_2$  error of the constructed surrogate model  $\tilde{f}$  defined by

$$\epsilon = \left( \int (f(\xi) - \tilde{f}(\xi))^2 d\nu_{S_2}(\xi) / \int f(\xi)^2 d\nu_{S_2}(\xi) \right)^{\frac{1}{2}}, \quad (4.12)$$

where 20 implementations were utilized for each training sample size number  $M$ . As shown in Figure 5(a),  $\tilde{f}(\xi)$  constructed by the near-orthonormal `amdP` basis yielded the smallest error while the tensor product of 380 Legendre basis functions yielded the largest error. Accordingly, the magnitudes of the recovered coefficients  $|\tilde{c}_i|$  by the exact and near-orthonormal bases decayed more quickly than those recovered using the Legendre basis functions, as shown in Figure 5(b). Furthermore,  $\tilde{f}(\xi)$  allowed us to define a new random vector  $\chi$ , which further enhanced the sparsity of  $\mathbf{c}$ , as shown in Figures 5(c) and (d). Following Step 5 in Algorithm 4, we defined a new random  $\chi$  through rotation. The associated representation coefficient vector  $\mathbf{c}$  has 385 enhanced sparsity.

However, for the exact and near-orthonormal basis, the  $\tilde{g}(\chi)$  gave smaller errors (the dashed curve) than  $\tilde{f}(\xi)$  (the solid curve), as shown in Figure 5(a). Thus, enhancing the sparsity of  $\mathbf{c}$  alone does not guarantee enhanced accuracy of  $\tilde{f}$ . In particular,  $\tilde{g}(\chi)$  constructed by the Legendre basis yielded larger error than  $\tilde{f}(\xi)$  as demonstrated in Figure 5(a); although, the sparsity of  $\mathbf{c}$  was greater, as seen in Figure 5(d). This behavior 390 indicates that retaining the orthonormal condition can be crucial for the accurate construction of  $\tilde{f}$ . The basis bound (see Table B.2 in Appendix B) provides a metric to understand why the near-orthonormal basis

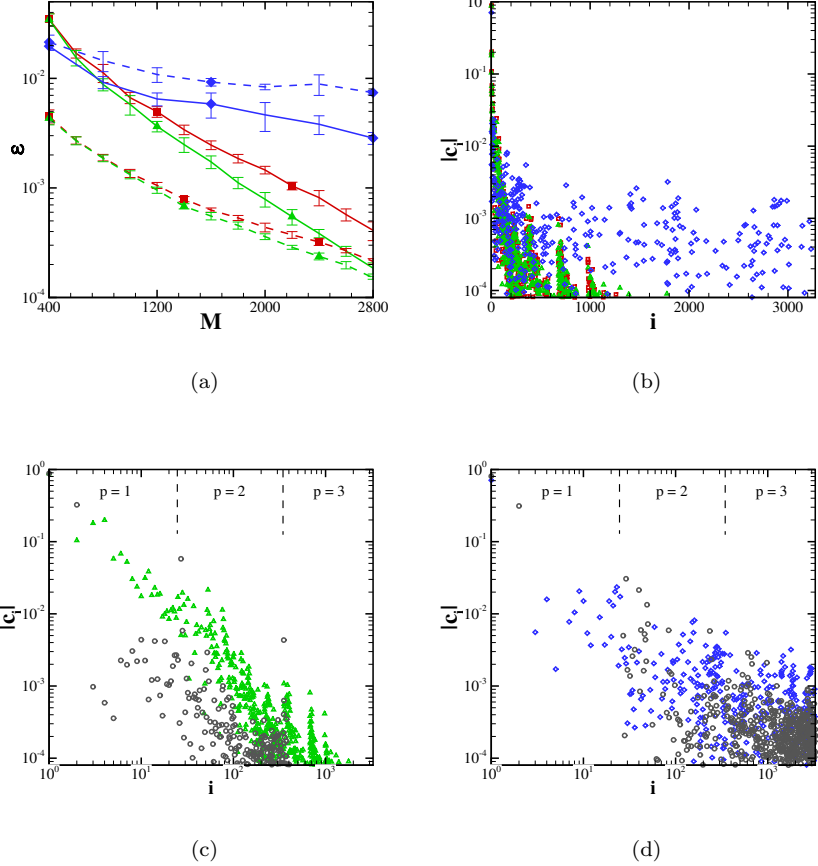


Figure 5: Numerical results for recovery of a high-dimensional polynomial function. The combination of near-orthonormal basis construction with the sparsity enhancement rotation procedure yields the most accurate results. Directly applying the rotation procedure to the Legendre basis may lead to increased error despite increased sparsity in  $\mathbf{c}$ . (a) Relative  $l_2$  error of the recovered polynomial function with different bases: the exact orthonormal  $\text{amdP}$  basis with respect to  $\xi$  (“ $\blacksquare$ ”) and  $\chi$  (“ $\blacksquare\blacksquare$ ”); the near-orthonormal  $\text{amdP}$  basis with respect to  $\xi$  (“ $\blacktriangle$ ”) and  $\chi$  (“ $\blacktriangle\blacktriangle$ ”); Legendre basis with respect to  $\xi$  (“ $\blacklozenge$ ”) and  $\chi$  (“ $\blacklozenge\blacklozenge$ ”). (b) Coefficients magnitude  $|c_i|$  recovered using different bases. “ $\blacksquare$ ”: the exact orthonormal  $\text{amdP}$  basis with respect to  $\xi$ ; “ $\blacktriangle$ ”: the near-orthonormal  $\text{amdP}$  basis with respect to  $\xi$ ; “ $\blacklozenge$ ”: Legendre basis with respect to  $\xi$ . (c) Recovered coefficient magnitude  $|c_i|$  using the near orthogonal basis with respect to  $\xi$  (“ $\blacktriangle$ ”) and  $\chi$  (“ $\circ$ ”). The dashed vertical lines indicate the separation between different polynomial orders  $p$ . (d) Recovered coefficient magnitude  $|c_i|$  using the Legendre basis with respect to  $\xi$  (“ $\blacklozenge$ ”) and  $\chi$  (“ $\circ$ ”).

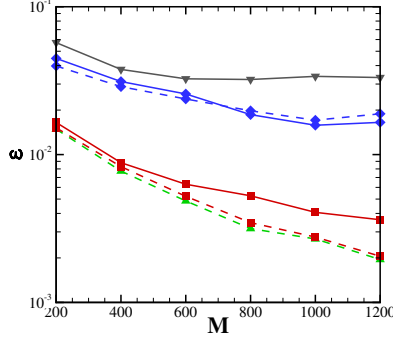


Figure 6: The combination of near-orthonormal basis construction and sparsity enhancement rotation yields the most accurate results, as shown through the relative  $l_2$  error of the constructed surrogate model for the 1D elliptic PDE with random permeability coefficient: the exact orthonormal `amdP` basis with respect to  $\xi$  (“ $\text{---} \blacksquare \text{---}$ ”) and  $\chi$  (“ $\text{---} \blacksquare \text{---}$ ”); Legendre basis with respect to  $\xi$  (“ $\text{---} \blacklozenge \text{---}$ ”) and  $\chi$  (“ $\text{---} \blacklozenge \text{---}$ ”); Hermite basis with respect to  $\xi$  (“ $\text{---} \blacktriangledown \text{---}$ ”); the near-orthonormal `amdP` basis with respect to  $\chi$  (“ $\text{---} \blacktriangle \text{---}$ ”).

performs better than the exact orthonormal basis.

#### 4.3.2. 1D elliptic PDEs with high-dimensional random inputs

In this example, we revisited the 1D elliptic PDE (4.7) with random coefficient given by Equation (4.9).

395 Here we set  $a_0(x) \equiv 1$ ,  $\sigma = 1$ ,  $l_c = 0.12$  and  $d = 20$  such that  $\sum_{i=1}^d \lambda_i > 0.91 \sum_{i=1}^\infty \lambda_i$ .

Similar to the work by Zabaras et al. [70], a non-Gaussian multivariate distribution was used for  $\xi = (\xi_1, \xi_2, \dots, \xi_d)$ . We generated a sample set  $\{\tilde{\xi}^{(k)}\}_{k=1}^{N_s}$ , where  $N_s = 2 \times 10^5$  and  $\tilde{\xi}$  came from the Gaussian mixture distribution specified in (4.1). We used PCA to transform  $\tilde{\xi}$  to  $\xi$  such that  $\mathbb{E}[\xi_i] = 0$  and  $\mathbb{E}[\xi_i \xi_j] = \delta_{ij}$ . For each input sample  $\xi^{(k)}$ ,  $a$  and  $u$  only depended on  $x$  and the solution of the deterministic elliptic equation is given by [54]

$$u(x) = u(0) + \int_0^x \frac{a(0)u(0)' - y}{a(y)} dy \quad (4.13)$$

$$a(0)u(0)' = \left( \int_0^1 \frac{y}{a(y)} dy \right) / \left( \int_0^1 \frac{1}{a(y)} dy \right).$$

We chose the QoI to be  $u(x; \xi)$  at  $x = 0.35$  and constructed a 3<sup>rd</sup>-order polynomial expansion with  $N = 1771$  basis functions. Figure 6 shows the relative  $l_2$  error of  $\tilde{f}(\xi)$  (solid curve) and  $\tilde{g}(\chi)$  (dashed curve) constructed by different bases. The data-driven bases (both exact orthonormal basis and near-orthonormal basis) showed more accurate results than the Legendre basis and the Hermite basis. In particular, the near-orthonormal basis with respect to the rotated variable  $\chi$  yielded the most accurate result (the green dashed curve). In contrast, directly employing the Legendre basis to the rotated variable  $\chi$  without reconstructing the basis function led to increased  $l_2$  error, although  $c$  shows more sparsity in terms of  $\chi$  (the gray dashed curve) than  $\xi$  (the gray solid curve).

#### 4.4. UQ study of a molecule system under Non-Gaussian conformational distributions

We demonstrated the proposed method on a physical system exploring conformational uncertainty in a small molecule system. Molecular properties, such as solvation energies or solvent-accessible surface areas (SASAs), are often calculated using single molecular conformations. However, due to thermal energy, a molecule undergoes conformational fluctuations which can induce significant uncertainty in properties calculated from single structures. Our previous work [1] was focused on quantifying this uncertainty using a simple multivariate Gaussian model for conformational fluctuations: the elastic network model [89]. However, it is well known that the conformational fluctuations are often non-Gaussian due to the complicated structure of the underlying energy landscape. Therefore, in the current study, we construct the data-driven basis *directly* from the samples of molecular trajectories collected from molecular dynamics (MD) simulations, thus eliminating the *over-simplified* Gaussian assumption.

We simulated the dynamics of the small molecule benzyl bromide under equilibrium (see Appendix E for details) and collected a sample set of the instantaneous molecular structure  $\{\mathbf{r}^{(k)}\}_{k=1}^{N_s}$  from MD simulation trajectories over  $20\mu\text{s}$ . In what follows,  $N_s = 2 \times 10^5$  and  $\mathbf{r}$  represent the positions of individual atoms. As a pre-processing step, we transformed  $\{\mathbf{r}^{(k)}\}_{k=1}^{N_s}$  into a set of uncorrelated random vectors  $S = \{\boldsymbol{\xi}^{(k)}\}_{k=1}^{N_s}$  via PCA:

$$\begin{aligned}\boldsymbol{\Sigma} &= \mathbb{E} \left[ (\mathbf{r} - \bar{\mathbf{r}})(\mathbf{r} - \bar{\mathbf{r}})^T \right] \\ \boldsymbol{\Sigma} &= \mathbf{Q}\boldsymbol{\Gamma}\mathbf{Q}^T \quad \boldsymbol{\xi} = \boldsymbol{\Gamma}^{-1/2}\mathbf{Q}^T\mathbf{r},\end{aligned}\tag{4.14}$$

where the average  $\mathbb{E}[\cdot]$  is taken over the entire sample set and  $\boldsymbol{\xi} \in \mathbb{R}^{12}$  is the normalized random vector that represents 99.99% of the observed variance. Figures 7(a) and (b) show the joint distributions of  $(\xi_1, \xi_2)$  and  $(\xi_1, \xi_3)$ . Although the individual components of  $\boldsymbol{\xi}$  are uncorrelated, the joint density distributions are mutually dependent and deviate from the standard Gaussian distributions.

We chose the polar solvation energy and SASA as the target QoIs for this system. The polar solvation energy was modeled by the Poisson-Boltzmann equation [90, 91]

$$-\nabla \cdot (\epsilon_f(\mathbf{x}; \boldsymbol{\xi}) \nabla \varphi(\mathbf{x}; \boldsymbol{\xi})) = \rho_f(\mathbf{x}; \boldsymbol{\xi})\tag{4.15}$$

which relates the electrostatic potential  $\varphi$  to a dielectric coefficient  $\epsilon_f$  and a fixed charge distribution  $\rho_f$ . Equation (4.15) is typically solved with Dirichlet boundary conditions set to an analytical asymptotic solution of the equation for an infinite domain. The dielectric coefficient  $\epsilon_f$  implicitly represents the boundary between the atoms of the molecule and the surrounding solvent: the coefficient changes rapidly across this boundary from a low dielectric value in the molecular interior to a high dielectric value in the solvent. The charge distribution  $\rho_f$  is generally modeled as a collection of  $\delta$ -like functions centered on the atoms of the molecule with magnitudes proportional to the atomic partial charges. Both  $\epsilon_f$  and  $\rho_f$  are dependent on the

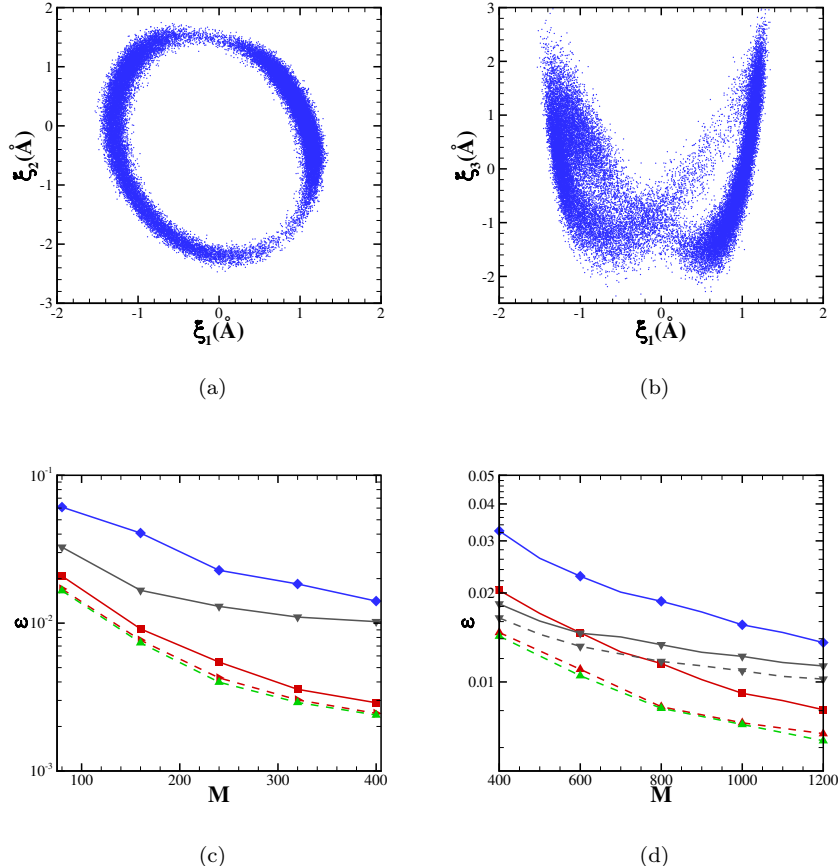


Figure 7: The present method based on data-driven basis construction and sparsity enhancement rotation yields the most accurate surrogate model for molecular systems with mutually dependent non-Gaussian density distributions. (a-b) Sampling points representing the joint distributions  $(\xi_1, \xi_2)$  (left) and  $(\xi_1, \xi_3)$  (right). (c-d) Relative  $l_2$  error of the polar solvation energy (left) and the local SASA (right) of an individual atom (the H9 atom attached to the ortho-carbon atom) obtained with different numbers of training data  $M$ : the exact  $\text{amdP}$  orthonormal basis with respect to  $\xi$  (“ $\blacksquare$ —”); Hermite basis with respect to  $\xi$  (“ $\blacktriangledown$ —”); Legendre basis with respect to  $\xi$  (“ $\blacklozenge$ —”); the near-orthonormal  $\text{amdP}$  basis with respect to  $\chi$  (“ $\blacktriangle$ —”).

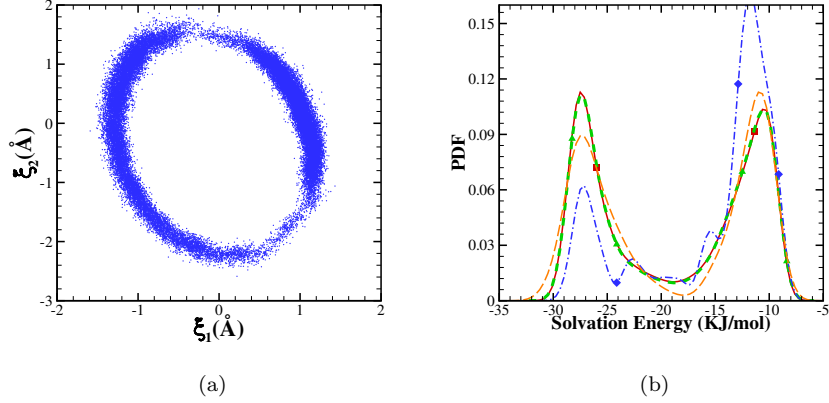


Figure 8: The present method yields the most accurate prediction on the PDF of the QoI for the molecular systems. Direct fitting of the underlying density  $\omega(\xi)$  using Gaussian Mixture model may induce biased error to the PDF prediction. (a) Fitted random variables  $(\xi_1, \xi_2)$  with Gaussian mixture models. (b) PDF of the solvation energy obtained with the Gaussian Mixture model and the present data-driven approach. “ $\text{---} \blacksquare \text{---}$ ”: reference solution obtained from  $2 \times 10^5$  MC samples; “ $\text{---} \blacklozenge \text{---}$ ”: direct MC sampling using the same set of 200 samples; “ $\text{---} \blacktriangle \text{---}$ ”: present method using the same set of 200 samples; “ $\text{---} \textcolor{orange}{\square} \text{---}$ ”: fitting Gaussian Mixture model using 800 samples.

instantaneous molecular structure (i.e.,  $\xi$ ). The polar solvation energy was calculated from

$$G_p(\xi) = \int \rho_f(\mathbf{x}; \xi) (\varphi(\mathbf{x}; \xi) - \varphi_h(\mathbf{x}; \xi)) d\mathbf{x} \quad (4.16)$$

where  $\varphi_h$  is a reference potential obtained from solution of

$$-\epsilon_h \nabla^2 \varphi_h(\mathbf{x}; \xi) = \rho_f(\mathbf{x}; \xi) \quad (4.17)$$

where  $\epsilon_h$  is a constant reference dielectric value. We used the Adaptive Poisson-Boltzmann Solver (APBS)  
420 software to solve the equations above [92]. Besides the solvation energy of the whole molecule, we also  
studied a local property like the SASA of an individual atom (the H9 atom attached to the ortho-carbon  
atom of the benzyl bromide molecule, see Figure E.11) by the Shake-Rupley algorithm [93] using APBS.  
Details of the APBS calculations are presented in Appendix E.

Figures 7(c) and (d) show the relative  $l_2$  error of the constructed surrogate model  $\tilde{f}(\xi)$  for the solvation  
425 energy and SASA using a 4<sup>th</sup>-order gPC expansion with  $N = 1820$  basis functions. For both QoIs, the near-  
orthonormal and orthonormal bases with respect to the rotated variable  $\chi$  (dashed curves) yield similar error  
which is much smaller than the error of Legendre and Hermite bases. A possible explanation for the similar  
performance of the near-orthonormal and orthonormal bases is the closeness of the basis bound estimates  
for these two bases (see Table B.3 in Appendix B).

Instead of the direct construction of  $\tilde{f}(\xi)$  using data-driven basis functions, another possible approach to  
430 characterize the uncertainty of the molecular system is to fit the distribution density  $\omega(\xi)$  with a distribution

model such as a Gaussian Mixture model. Figure 8 (a) shows a scatter plot of the joint distribution  $(\xi_1, \xi_2)$  extracted from the fitted Gaussian mixture distribution  $\tilde{\omega}(\xi)$  using 7 Gaussian modes. Accordingly, we can construct the surrogate model for each Gaussian mode using standard Hermite basis function. However, it is well-known that accurate construction of  $\omega(\xi)$  is a numerically challenging problem for  $d > 4$ . As shown in Figure 8(b), direct fitting  $\omega(\xi)$  by  $\tilde{\omega}(\xi)$  induces non-negligible error and leads to biased prediction of the PDF of the solvation energy. Furthermore, we lose the one-to-one mapping between the individual conformation state  $\xi$  and the QoIs through the constructed surrogate model  $\tilde{f}(\xi)$ .

## 5. Summary

In this study, we have developed a DSRAR framework for constructing surrogate models irrespective of the mutual dependence between the components of random inputs using limited training points. To the best of our knowledge, this problem has not been addressed by previous UQ studies based on polynomial chaos expansions. The DSRAR framework does not assume mutual independence between the components of random inputs and therefore can be applied to UQ in complex systems where information about the underlying random distribution can be implicit. To construct the surrogate model, this framework uses data-driven `amdP` basis construction and a sparsity-enhancing rotation procedure which leads to more accurate recovery of the sparse representation of the target function. The method benefits from both the orthonormal basis expansion and the enhanced sparsity of the expansion coefficients. With the assumption that there exists a sparse representation of the surrogate model, the DSRAR approach can be applied to challenging UQ problems under two widely encountered situations: (I) probability measure implicitly represented by a large collection of samples and (II) non-Gaussian probability measures with explicit (analytical) forms. For systems with explicit knowledge of the probability measure, our method exploits sparser representations of QoIs while retaining proper orthogonality with respect to rotated variables. For systems with randomness implicitly represented by a large collection of random samples, we also proposed a heuristic method to construct a *near-orthonormal* basis in addition to the exact orthonormal basis with respect to the discrete measure. The near-orthonormal basis shows a smaller basis bound and empirically yields more accurate representations. The numerical examples show the effectiveness of our method for realistic problems on quantifying uncertainty propagation in molecular system under conformational fluctuations as well as PDEs with arbitrary underlying probability measures.

For future study, we note that several issues not considered in the present work could further improve the performance of the present DSRAR framework. The heuristic approach to constructing near-orthonormal basis introduced in this study yields smaller basis bounds and more accurate representations than existing methods. However, we do not have the theoretical analysis to formally show that the near-orthonormal basis is optimal and to establish the conditions under which it outperforms the exact orthonormal basis. It

would be interesting to investigate different approaches of data-driven basis construction to further improve the properties of measurement matrix for CS purposes. For instance, if new data becomes available after the surrogate construction, it is worth exploring how to use the new information to design more sophisticated (cross-validation) strategies to optimize the orthonormal threshold values and the basis construction procedure. Furthermore, our study used a standard  $\ell_1$  minimization approach for relaxing the CS problem and recovering a sparse solution of the under-determined system. However, other optimization approaches can be employed when the measurement matrix is highly coherent when  $\ell_1$  minimization is not necessarily optimal. Finally, it would be interesting to employ the developed DSRAR approach for UQ study in other complex biological systems [94, 95]. Such results will be presented in a future publication.

## Appendix A. Proof of Theorem 4.1

*Proof.* Let  $\mathbf{v} \in \text{Ker } \mathbf{A}$  and  $\mathbf{x} \neq \mathbf{c}$  another solution of  $\mathbf{Ax} = \mathbf{b}$ . To show that  $\mathbf{c}$  is the unique  $\ell_1$  minimizer of  $\mathbf{Ac} = \mathbf{b}$ , it is sufficient if

$$\|\mathbf{v}_{T_\alpha}\|_1 < \|\mathbf{v}_{T_\alpha^c}\|_1, \quad (\text{A.1})$$

which gives

$$\begin{aligned} \|\mathbf{c}\|_1 &\leq \|\mathbf{c} - \mathbf{x}_{T_\alpha}\|_1 + \|\mathbf{x}_{T_\alpha}\|_1 = \|\mathbf{c}_{T_\alpha} - \mathbf{x}_{T_\alpha}\|_1 + \|\mathbf{x}_{T_\alpha}\|_1 = \|\mathbf{v}_{T_\alpha}\|_1 + \|\mathbf{x}_{T_\alpha}\|_1 \\ &< \|\mathbf{v}_{T_\alpha^c}\|_1 + \|\mathbf{x}_{T_\alpha}\|_1 = \|\mathbf{x}\|_1. \end{aligned} \quad (\text{A.2})$$

To satisfy (A.1), we partition  $T_\alpha^c$  into  $T_\alpha^c = T_{\alpha,1}^c \cup T_{\alpha,2}^c \cup \dots$ , where  $T_{\alpha,1}^c$  is the index set of  $s$  largest absolute entries of  $\mathbf{v}$  in  $T_\alpha^c$ ,  $T_{\alpha,2}^c$  is the index set of  $s$  largest absolute entries of  $\mathbf{v}$  in  $T_\alpha^c \setminus T_{\alpha,1}^c$ . Accordingly,

$$\|\mathbf{v}_{T_\alpha}\|_2^2 \leq \frac{1}{1-\delta_s} \|\mathbf{Av}_{T_\alpha}\|_2^2 = \frac{1}{1-\delta_s} \sum_{k=1} \langle \mathbf{Av}_{T_\alpha}, \mathbf{A}(-\mathbf{v}_{T_{\alpha,k}^c}) \rangle \leq \frac{\theta_s}{1-\delta_s} \sum_{k=1} \|\mathbf{v}_{T_\alpha}\|_2 \|\mathbf{v}_{T_{\alpha,k}^c}\|_2, \quad (\text{A.3})$$

which gives  $\|\mathbf{v}_{T_\alpha}\|_2 \leq \frac{\theta_s}{1-\delta_s} \sum_{k=1} \|\mathbf{v}_{T_{\alpha,k}^c}\|_2$ . The remaining of the proof is straightforward and follows Theorem 2.6 of Rauhut [96]. By the Cauchy-Schwarz inequality, we obtain

$$\|\mathbf{v}_{T_\alpha}\|_1 \leq \frac{\theta_s}{1-\delta_s} (\|\mathbf{v}_{T_\alpha}\|_1 + \|\mathbf{v}_{T_\alpha^c}\|_1). \quad (\text{A.4})$$

Equation (A.1) follows if  $\frac{\theta_s}{1-\delta_s} < 0.5$ . □

**Remark Appendix A.1.** We emphasize that Theorem 4.1 holds only for the given index set  $T_\alpha$ ; it provides a metric to examine the recovery accuracy with respect to measurement matrix  $\mathbf{A}$  and should not be viewed as the sufficient condition for exact recovery of *arbitrary s-sparse vector* via  $\ell_1$ -minimization (see canonical references [82, 83, 96] for details). Theorem 4.1 also indicates that, for the given index set  $T_\alpha$ , small  $\|\mathbf{A}_{T_\alpha}^* \mathbf{A}_{T_\alpha} - I\|_2$  will promote the recover of  $\mathbf{v}_{T_\alpha}$ .

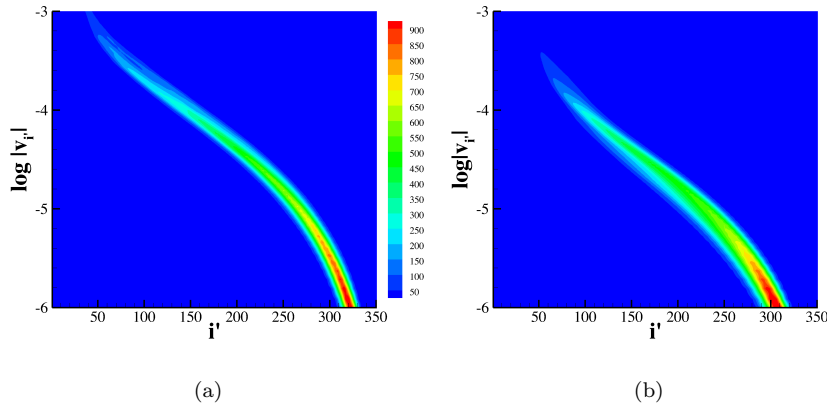


Figure B.9: The null spaces of measurement matrices constructed by the exact and near-orthonormal bases are different under  $\|v_{T_\alpha}\|_1 > \|v_{T_\alpha^c}\|_1$ —a necessary condition for  $c$  not being recoverable exactly. Density contour of the normalized null space vector component  $\log |v_i|$  (sorted by magnitude) of the measurement matrix  $A$  constructed by orthogonal (a) and near-orthogonal basis functions (b) that satisfy  $\|v_{T_\alpha}\|_1 > \|v_{T_\alpha^c}\|_1$  and  $\|v\|_2 = 1$ .

## Appendix B. Measurement matrix and basis bounds

### *Appendix B.1. Null space of measurement matrix from Section 4.1*

Let  $\tilde{\mathbf{c}} = \mathbf{c} + \mathbf{v}$ ,  $\mathbf{v} \in \text{Ker } \mathbf{A}$  where  $\mathbf{A}$  is the measurement matrix defined in (4.3). From the null space property [96],  $\tilde{\mathbf{c}}$  does not fully recover  $\mathbf{c}$  by  $\ell_1$  minimization (i.e., equation (2.6)) only if  $\|\tilde{\mathbf{c}}\|_1 < \|\mathbf{c}\|_1$ . As a *necessary condition* for the failure of recovery, it requires

$$\|v_{T_\alpha}\|_1 > \|v_{T_\alpha^c}\|_1, \quad (\text{B.1})$$

where  $T_\alpha^c$  refers to the complement of  $T_\alpha$ . Accordingly, different null space of measurement matrix  $A$  generally leads to different recovery error.

We examined the above necessary condition (B.1) for different measurement matrices by randomly choosing a non-zero index set  $T_\alpha$  with  $|T_\alpha| = 50$  and  $M = 180$ . For  $\mathbf{A}$  constructed by both basis sets, we collected 1000 normalized  $\mathbf{v} \in \text{Ker } \mathbf{A}$  that satisfy  $\|\mathbf{v}_{T_\alpha}\|_1 > \|\mathbf{v}_{T_\alpha^c}\|_1$ . Figure B.9 shows the density contour of individual component  $|\mathbf{v}_{i'}|$  in log-scale, where  $i'$  refers to the index sorted by magnitude in descending order. The two basis sets demonstrate different distributions of  $\log |\mathbf{v}_{i'}|$ , which likely contribute to the different recovery errors shown in Figure 2.

## Appendix B.2. Basis bounds

The lower bound of the required number of samples  $M$  given in Theorem 2.5 suggests that bases with smaller basis bounds  $K$  are preferred. We expect that smaller basis bounds will correlate with higher

accuracy representations. For the constructed basis set  $\psi_i(\xi), i = 1, \dots, N$ , we define the basis bound  $\tilde{K}$  on the given data set  $S$  by

$$\tilde{K} := \frac{1}{|S_{M_\sigma}|} \sum_{\xi \in S_{M_\sigma}} |k(\xi)|, \quad (\text{B.2})$$

where the set  $S_{M_\sigma}$  is defined by  $S_{M_\sigma} = \{\xi \mid |k(\xi) - \mathbb{E}[k]| > M_\sigma \sigma[k], \xi \in S\}$ . Here  $k(\xi) := \max_i |\psi_i(\xi)|$  denotes the maximum magnitude for an individual sampling point  $\xi$ ,  $\mathbb{E}[k]$  and  $\sigma[k]$  represent the mean and the standard deviation of  $k(\xi)$  on  $S$  with respect to the discrete measure  $\nu_S$ . In this study, we present  $\tilde{K}$  as an indication of the difference between the exact and near-orthonormal basis function. In compressive sensing, the measurement matrix only consists of limited number of samples. Therefore, we employ the mean of the tails in the basis bounds as an indicator of the upper bound of the largest entry values from the measurement matrix.  $M_\sigma$  defines the range of this tail set. We choose  $M_\sigma = 5$  if not specified otherwise.

Table B.1:  $\tilde{K}$  of constructed basis set for Gaussian mixture system  $d = 25$ ,  $p = 2$  and  $N_s = 1 \times 10^5$ .

$M_\sigma$	3	4	5	6	$\max_{\xi \in S} k(\xi)$
$\tilde{K}_{\text{orth}}$	10.359	12.048	13.895	15.513	22.208
$\tilde{K}_{\text{near-orth}}$	9.622	11.196	12.867	14.448	18.790

Following the definition by Equation (B.2), we examine the basis bound  $\tilde{K}$  of the numerical examples presented in this study. Table B.1 shows the results of Gaussian mixture system  $\{\xi^{(i)}\}, i = 1, \dots, N_s$  with  $N_s = 1 \times 10^5$ ,  $d = 25$  and  $p = 2$  which is defined in Section 4.1. For different values of  $M_\sigma$ ,  $\tilde{K}$  of the near orthogonal basis shows consistently smaller values than the values of the exact orthogonal basis set.

Table B.2 shows the basis bound  $\tilde{K}$  of the Gaussian mixture system which is studied in Section 4.3.1 with  $N_s = 2 \times 10^5$ ,  $d = 25$  and  $p = 3$ . The values of  $\tilde{K}$  for the near orthogonal basis are consistently smaller than the value for the exact orthogonal basis set no matter on the original random sample set or the rotated sample set. Furthermore, we present the basis bounds on the rotated sampling set  $\{\chi_M^{(i)}\}_{i=1}^{N_s}$ , where the subscript “ $M$ ” refers to the different number of training points utilized to construct the surrogate model  $X(\xi)$ . The near-orthogonal basis yields smaller  $\tilde{K}$  than the exact orthogonal basis in each case.

Similarly, Table B.3 shows  $\tilde{K}$  of the constructed basis for uncertainty quantification of the molecular solvation energy ( $d = 12$ ,  $p = 4$  and  $N_s = 2 \times 10^5$ ), which is studied in Section 4.4. The near-orthogonal basis yields smaller values consistently for different number ( $\chi_M$ ) of training points.

## Appendix C. Other metrics for the surrogate model

Besides the relative  $l_2$  error, we have also computed the predictivity coefficients  $Q_2$  for the test cases of Gaussian mixture (with  $d = 25$  and  $p = 3$ ) and molecular systems. Similar to Marrel et al. [97],  $Q_2$  is defined

Table B.2:  $\tilde{K}$  of constructed basis set for Gaussian mixture system  $d = 25$ ,  $p = 3$  and  $N_s = 2 \times 10^5$ .

	$\xi$	$\chi_{M=400}$	$\chi_{M=1200}$	$\chi_{M=1600}$	$\chi_{M=2400}$
$\tilde{K}_{\text{orth}}$	32.497	32.522	32.079	33.142	32.308
$\tilde{K}_{\text{near-orth}}$	28.320	29.811	29.407	29.512	29.192

 Table B.3:  $\tilde{K}$  of constructed basis set for molecular system  $d = 12$ ,  $p = 4$  and  $N_s = 2 \times 10^5$ .

	$\chi_{M=80}$	$\chi_{M=160}$	$\chi_{M=240}$	$\chi_{M=320}$	$\chi_{M=400}$
$\tilde{K}_{\text{orth}}$	40.596	39.914	39.789	39.218	39.142
$\tilde{K}_{\text{near-orth}}$	39.970	39.278	39.290	38.528	38.631

by

$$Q_2 = 1 - \int (f(\xi) - \bar{f}(\xi))^2 d\nu_{S_2}(\xi) / \int (f(\xi) - \bar{f})^2 d\nu_{S_2}(\xi), \quad (\text{C.1})$$

where  $\bar{f}$  represents the mean of QoI on  $S_2$ . The results are shown in Tab. C.4, where the surrogate models are constructed by the our data-driven basis approach.

 Table C.4: The predictivity coefficient  $Q_2$  for polynomial function with Gaussian Mixture measure ( $d = 25$  and  $p = 3$ ) and the molecular system for solvation energy and SASA of atom H9.

molecule solvation	$M$	80	160	240	320	400
	$Q_2$	0.995715	0.999132	0.999731	0.999864	0.999911
molecule SASA	$M$	200	300	400	500	600
	$Q_2$	0.988675	0.996069	0.998272	0.998709	0.999027
Gaussian Mixture	$M$	200	300	400	500	600
	$Q_2$	0.998372	0.999347	0.999844	0.999892	0.999941

With the constructed surrogate model, we can compute the Sobol' sensitivity indices for QoI with dependent random variables. In brief,  $f(\xi)$  is expanded by

$$f(\xi) = \eta_0(\xi) + \sum_{\beta \in \Theta^d} \eta_\beta(\xi), \quad (\text{C.2})$$

where  $\Theta^d$  represents the collection of all subsets of  $[1 : d]$  and  $\eta_\beta(\xi)$  satisfies  $\mathbb{E}[\eta_\alpha, \eta_\beta] = 0$ , if  $\alpha \subset \beta$ . The sensitivity index  $S_\beta$  is given by

$$S_\beta = \frac{\mathbb{V}(\eta_\beta) + \sum_{\alpha \cap \beta \neq \alpha, \beta} \text{Cov}(\eta_\alpha, \eta_\beta)}{\mathbb{V}(f)} \quad (\text{C.3})$$

where  $\mathbb{V}(\cdot)$  refers to the variance on  $\nu_S$ . We refer to Chastaing et al. [98] for the details. Fig. C.4 shows the first-order sensitivity indices for the test cases of Gaussian mixture systems ( $d = 25$ ,  $p = 3$ ) and the

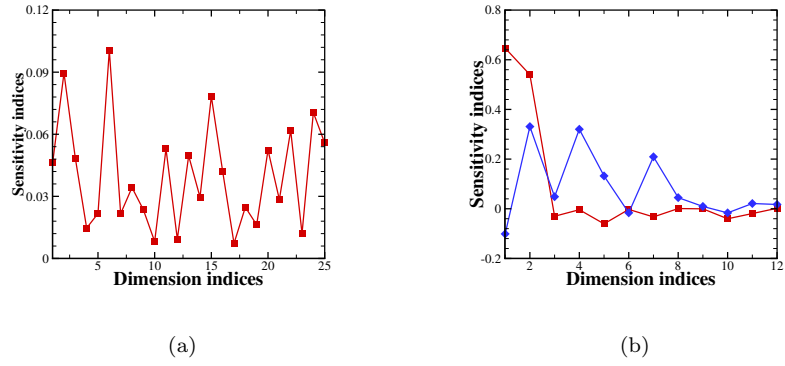


Figure C.10: The first-order Sobol' sensitivity indices for (a) polynomial function with Gaussian mixture measure ( $d = 25$ ,  $p = 3$ ) (b) molecular system for solvation energy (“ $\text{---} \blacksquare \text{---}$ ”) and SASA of atom H9(“ $\text{---} \blacklozenge \text{---}$ ”).

molecular systems, where the surrogate models are constructed by the data-driven basis approach using  $M = 800$ ,  $M = 240$  and  $M = 600$  training points, respectively. The dominant components are on the dimensions  $(1, 2, 3, 6, 11, 13, 14, 15, 16, 20, 22, 24, 25)$ ,  $(1, 2, 5)$  and  $(1, 2, 4, 5, 7)$  (90% of total variance).

## 520 Appendix D. Generation of the Gaussian mixture data set

We used Matlab to generate the Gaussian mixture data set in Sec. 4.1 by calling the function `gmdistribution( $\mu$ ,  $\{\Sigma_i\}_{i=1}^3, a$ )` with  $a = (0.5358, 0.1281, 0.3361)$ .  $\mu$  is a  $25 \times 3$  random matrix with i.i.d. entries on  $U[-2.5, 2.5]$ .  $\{\Sigma_i\}_{i=1}^3$  is a  $25 \times 25 \times 3$  array where  $\Sigma_i$  is defined by

$$\Sigma_i = (\Upsilon_i \Upsilon_i^T + I)/4, \quad (\text{D.1})$$

where  $\Upsilon_i$  is a random matrix with i.i.d. entries from  $\mathcal{U}[0, 1]$  for  $i = 1, 2, 3$ .  $\mu$  and  $\Upsilon_i$  are generated by calling the Matlab function `rand()` with random number seed 200.

## Appendix E. Molecular Dynamics simulation and calculation details

We performed all-atom MD simulation of benzyl bromide in water using GROMACS 5.1.2 [99]. The 525 simulation system included a benzyl bromide molecule (see Figure E.11 for the molecular structure) and 1011 water molecules. The General AMBER Force Field (GAFF) [100] was used for the benzyl bromide parameters. The partial charges of benzyl bromide molecule were calculated by RESP method [101]. Bond lengths of benzyl bromide were constrained using the LINCS algorithm [102]. The water molecule was modeled with the rigid TIP3P water model [103]. The bond lengths and angles were held constant through 530 the SETTLE algorithm [104]. The system was equilibrated in the isothermal-isobaric ensemble for 10 ns at 300K and 1 bar after energy minimization. The van der Waals cut-off radii was 1.0 nm. Long-range

electrostatics were calculated using a Particle Mesh Ewald (PME) summation with grid spacing of 0.12 nm. The time step was 2 fs. Isobaric-isothermal simulations were equilibrated using a V-rescale thermostat and Berendsen barostat. Following equilibration, the simulation was run for a production period of 20  $\mu$ s in a  
535 NVT ensemble with a Nosé-Hoover thermostat. The trajectory was stored every 10000 time steps.

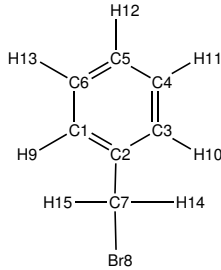


Figure E.11: Sketch of the molecule benzyl bromide with labeled atoms.

APBS calculations [105, 92] were performed with  $129^3$  grid points over a  $40 \times 40 \times 40 \text{ \AA}^3$  coarse grid domain with focusing to a  $14 \times 14 \times 14 \text{ \AA}^3$  fine grid domain with the grid origin located at the geometric center of the molecule. The Poisson equation was solved with Dirichlet boundary conditions based on the asymptotic behavior of multiple point charges in a homogeneous dielectric medium. The dielectric coefficient  
540 inside the domain used a van der Waals molecular volume definition with a dielectric value of 2.0 inside the molecule and 78.0 outside the molecule. Charges were modeled by Dirac delta functions but discretized to the finite difference grid points using a cubic spline approximation.

## Acknowledgements

We thank Ling Guo (Shanghai Normal University), Lei Wu (Princeton University), Wen Zhou (Colorado  
545 State University), and David Sept (University of Michigan, ORCID:0000-0003-3719-2483) for helpful discussions. This work was supported by the U.S. Department of Energy, Office of Science, Office of Advanced Scientific Computing Research as part of the Collaboratory on Mathematics for Mesoscopic Modeling of Materials (CM4) and by the National Institutes of Health grant R01 GM069702. The research was performed using resources available through Research Computing at Pacific Northwest National Laboratory HL  
550 acknowledges grant support from AMS Simons Post-doctoral Travel Grant and PNNL Laboratory Directed Research & Development (LDRD) under project “Development of physics-compatible stochastic models for multiphysics systems”.

## References

- [1] H. Lei, X. Yang, B. Zheng, G. Lin, N. A. Baker, Constructing surrogate models of complex systems with enhanced sparsity: Quantifying the influence of conformational uncertainty in biomolecular solvation,

- SIAM Multiscale Model. Simul. 13 (4) (2015) 1327–1353.
- [2] S. Oladyshkin, W. Nowak, Data-driven uncertainty quantification using the arbitrary polynomial chaos expansion, Reliability Engineering & System Safety 106 (2012) 179 – 190.
- [3] A. Saltelli, [Global sensitivity analysis: the primer](#), John Wiley, 2008.
- [4] C. M. Bishop, [Pattern Recognition and Machine Learning \(Information Science and Statistics\)](#), Springer-Verlag, Berlin, Heidelberg, 2006.
- [5] A. Laio, M. Parrinello, Escaping free-energy minima, Proceedings of the National Academy of Sciences 99 (20) (2002) 12562–12566.
- [6] G. Fishman, Monte Carlo: Concepts, Algorithms, and Applications, Springer-Verlag New York, Inc., 1996.
- [7] S. Kucherenko, D. Albrecht, A. Saltelli, [Exploring multi-dimensional spaces: a Comparison of Latin Hypercube and Quasi Monte Carlo Sampling Techniques](#) (2015). [arXiv:arXiv:1505.02350](#).
- [8] M. B. Giles, [Multilevel Monte Carlo methods](#), Acta Numerica 24 (2015) 259 – 328.
- [9] S. Heinrich, [Multilevel Monte Carlo Methods](#), in: S. Margenov, J. Waśniewski, P. Yalamov (Eds.), Large-Scale Scientific Computing, Springer Berlin Heidelberg, Berlin, Heidelberg, 2001, pp. 58–67.
- [10] M. Pisaroni, F. Nobile, P. Leyland, [A Continuation Multi Level Monte Carlo \(C-MLMC\) method for uncertainty quantification in compressible inviscid aerodynamics](#), Computer Methods in Applied Mechanics and Engineering 326 (2017) 20 – 50.
- [11] P. Koutsourelakis, [Accurate Uncertainty Quantification Using Inaccurate Computational Models](#), SIAM Journal on Scientific Computing 31 (5) (2009) 3274–3300.
- [12] B. Peherstorfer, K. Willcox, M. Gunzburger, [Optimal Model Management for Multifidelity Monte Carlo Estimation](#), SIAM Journal on Scientific Computing 38 (5) (2016) A3163–A3194.
- [13] B. Fox, Strategies for Quasi-Monte Carlo, Kluwer Academic Pub., 1999.
- [14] H. Niederreiter, Random number generation and Quasi-Monte Carlo methods, SIAM, 1992.
- [15] H. Niederreiter, P. Hellekalek, G. Larcher, P. Zinterhof, Monte Carlo and Quasi-Monte Carlo methods 1996, Springer-Verlag, 1998.
- [16] M. D. McKay, R. J. Beckman, W. J. Conover, [Comparison of Three Methods for Selecting Values of Input Variables in the Analysis of Output from a Computer Code](#), Technometrics 21 (2) (1979) 239–245.

- [17] M. Stein, Large sample properties of simulations using Latin Hypercube Sampling, *Technometrics* 29 (2) (1987) 143–151.
- [18] W. Loh, On Latin hypercube sampling, *Ann. Stat.* 24 (5) (1996) 2058–2080.
- [19] J. Sacks, W. J. Welch, T. J. Mitchell, H. P. Wynn, [Design and Analysis of Computer Experiments](#), *Statist. Sci.* 4 (4) (1989) 409–423.
- [20] M. C. Kennedy, A. O'Hagan, [Bayesian calibration of computer models](#), *Journal of the Royal Statistical Society: Series B (Statistical Methodology)* 63 (3) (2001) 425–464.
- [21] C. Rasmussen, C. Williams, [Gaussian Processes for Machine Learning](#), Adaptive Computation and Machine Learning, MIT Press, Cambridge, MA, USA, 2006.
- [22] N. Wiener, The homogeneous chaos, *Amer. J. Math.* 60 (1938) 897–936.
- [23] R. Ghanem, P. Spanos, Stochastic Finite Elements: A Spectral Approach, Springer-Verlag, 1991.
- [24] D. Xiu, G. E. Karniadakis, The wiener-askey polynomial chaos for stochastic differential equations, *SIAM J. Sci. Comput.* 24 (2002) 619–644.
- [25] P. Z. G. Qian, C. F. J. Wu, [Bayesian Hierarchical Modeling for Integrating Low-Accuracy and High-Accuracy Experiments](#), *Technometrics* 50 (2) (2008) 192–204.
- [26] B. Williams, D. Higdon, J. Gattiker, L. Moore, M. McKay, S. Keller-McNulty, [Combining experimental data and computer simulations, with an application to flyer plate experiments](#), *Bayesian Anal.* 1 (4) (2006) 765–792. doi:10.1214/06-BA125.
- [27] J. Oakley, A. O'Hagan, [Bayesian inference for the uncertainty distribution of computer model outputs](#), *Biometrika* 89 (4) (2002) 769–784.
- [28] B. A. Lockwood, M. Anitescu, [Gradient-Enhanced Universal Kriging for Uncertainty Propagation](#), *Nuclear Science and Engineering* 170 (2) (2012) 168–195. doi:10.13182/NSE10-86.
- [29] D. Xiu, G. Karniadakis, Modeling uncertainty in flow simulations via generalized polynomial chaos, *J. Comput. Phys.* 187 (2003) 137–167.
- [30] R. Ghanem, S. Masri, M. Pellissetti, R. Wolfe, Identification and prediction of stochastic dynamical systems in a polynomial chaos basis, *Comput. Meth. Appl. Math. Engrg.* 194 (2005) 1641–1654.
- [31] O. Knio, O. Le Maître, Uncertainty propagation in CFD using polynomial chaos decomposition, *Fluid Dyn. Res.* 38 (9) (2006) 616–640.

- [32] B. Sudret, Global sensitivity analysis using polynomial chaos expansions, *Reliability Engineering & System Safety* 93 (7) (2008) 964 – 979.
- [33] J. Li, D. Xiu, A generalized polynomial chaos based ensemble Kalman filter with high accuracy, *J. Comput. Phys.* 228 (2009) 5454–5469.
- [34] Y. Marzouk, D. Xiu, A stochastic collocation approach to bayesian inference in inverse problems, *Communications in Computational Physics* 6 (4) (2009) 826–847. doi:10.4208/cicp.2009.v6.p826.
- [35] J. Li, D. Xiu, Evaluation of failure probability via surrogate models, *J. Comput. Phys.* 229 (2010) 8966–8980.
- [36] J. Li, P. Stinis, Mori-zwanzig reduced models for uncertainty quantification, arXiv:1803.02826.
- [37] R. Schobi, B. Sudret, J. Wiart, [Polynomial-chaos-based Kriging](#), *International Journal for Uncertainty Quantification* 5 (2) (2015) 171–193.
- [38] L. L. Gratiet, S. Marelli, B. Sudret, [Metamodel-Based Sensitivity Analysis: Polynomial Chaos Expansions and Gaussian Processes](#), Springer International Publishing, Cham, 2016, pp. 1–37.
- [39] N. Owen, P. Challenor, P. Menon, S. Bennani, [Comparison of Surrogate-Based Uncertainty Quantification Methods for Computationally Expensive Simulators](#), *SIAM/ASA Journal on Uncertainty Quantification* 5 (1) (2017) 403–435. doi:10.1137/15M1046812.
- [40] P. T. Roy, N. El Moçayd, S. Ricci, J.-C. Jouhaud, N. Goutal, M. De Lozzo, M. C. Rochoux, [Comparison of polynomial chaos and Gaussian process surrogates for uncertainty quantification and correlation estimation of spatially distributed open-channel steady flows](#), *Stochastic Environmental Research and Risk Assessment* 32 (6) (2018) 1723–1741.
- [41] L. Mathelin, M. Hussaini, A stochastic collocation algorithm for uncertainty analysis, *Tech. Rep. NASA/CR-2003-212153*, NASA Langley Research Center (2003).
- [42] D. Xiu, J. Hesthaven, High-order collocation methods for differential equations with random inputs, *SIAM J. Sci. Comput.* 27 (3) (2005) 1118–1139.
- [43] I. Babuška, F. Nobile, R. Tempone, A stochastic collocation method for elliptic partial differential equations with random input data, *SIAM J. Numer. Anal.* 45 (3) (2007) 1005–1034.
- [44] F. Nobile, R. Tempone, C. G. Webster, A sparse grid stochastic collocation method for partial differential equations with random input data, *SIAM J. Numer. Anal.* 46 (5) (2008) 2309–2345.

- [45] X. Ma, N. Zabaras, An adaptive hierarchical sparse grid collocation algorithm for the solution of stochastic differential equations, *J. Comput. Phys.* 228 (8) (2009) 3084–3113.
- [46] J. Foo, G. E. Karniadakis, Multi-element probabilistic collocation method in high dimensions, *J. Comput. Phys.* 229 (5) (2010) 1536 – 1557.
- [47] P. G. Constantine, M. S. Eldred, E. T. Phipps, Sparse pseudospectral approximation method, *Computer Methods in Applied Mechanics and Engineering* 229-232 (2012) 1 – 12. doi:<https://doi.org/10.1016/j.cma.2012.03.019>.
- [48] J. D. Jakeman, S. G. Roberts, Local and dimension adaptive stochastic collocation for uncertainty quantification, in: *Sparse grids and applications*, Springer, 2013, pp. 181–203.
- [49] J. Li, P. Stinis, A unified framework for mesh refinement in random and physical space, *Journal of Computational Physics* 323 (2016) 243 – 264. doi:<https://doi.org/10.1016/j.jcp.2016.07.027>.
- [50] A. Doostan, H. Owhadi, A non-adapted sparse approximation of pdes with stochastic inputs, *J. Comput. Phys* 230 (2011) 3015–3034.
- [51] L. Yan, L. Guo, D. Xiu, Stochastic collocation algorithms using  $\ell^1$  minimization, *Inter. J. Uncertain Quantification* 2 (2012) 279–293.
- [52] H. Rauhut, R. Ward, Sparse legendre expansions via  $\ell_1$ -minimization, *J. Approx. Theory* 164 (2012) 517–533.
- [53] L. Mathelin, K. A. Gallivan, A compressed sensing approach for partial differential equations with random input data, *Communications in Computational Physics* 12 (4) (2012) 919?954. doi:[10.4208/cicp.151110.090911a](https://doi.org/10.4208/cicp.151110.090911a).
- [54] X. Yang, G. E. Karniadakis, Reweighted  $\ell_1$  minimization method for stochastic elliptic differential equations, *J. Comput. Phys.* 248 (2013) 87–108.
- [55] J. Hampton, A. Doostan, Compressive sampling of polynomial chaos expansions: Convergence analysis and sampling strategies., *J. Comput. Phys* 280 (2015) 363–386.
- [56] J. Peng, J. Hampton, A. Doostan, On polynomial chaos expansion via gradient-enhanced  $\ell_1$ -minimization, *J. Comput. Phys* 310 (2016) 440–458.
- [57] L. Yan, Y. Shin, D. Xiu, Sparse approximation using  $\ell_1 - \ell_2$  minimization and its application to stochastic collocation, *SIAM Journal on Scientific Computing* 39 (1) (2017) A229–A254. doi:[10.1137/15M103947X](https://doi.org/10.1137/15M103947X).

- [58] Y. L. Liu, L. Guo, Stochastic collocation via l1-minimisation on low discrepancy point sets with application to uncertainty quantification, *EAJAM* 6 (2016) 171–191.
- [59] H. Lei, X. Yang, Z. Li, G. E. Karniadakis, Systematic parameter inference in stochastic mesoscopic modeling, *J. Comput. Phys.* 330 (4) (2017) 571–593.
- [60] N. Alemazkoor, H. Meidani, Divide and conquer: An incremental sparsity promoting compressive sampling approach for polynomial chaos expansions, *Computer Methods in Applied Mechanics and Engineering* 318 (2017) 937 – 956. doi:<https://doi.org/10.1016/j.cma.2017.01.039>.
- [61] P. Diaz, A. Doostan, J. Hampton, Sparse polynomial chaos expansions via compressed sensing and d-optimal design, *Computer Methods in Applied Mechanics and Engineering* 336 (2018) 640 – 666. doi:<https://doi.org/10.1016/j.cma.2018.03.020>.
- [62] P. Rai, K. Sargsyan, H. Najm, Compressed sparse tensor based quadrature for vibrational quantum mechanics integrals, *Computer Methods in Applied Mechanics and Engineering* 336 (2018) 471 – 484. doi:<https://doi.org/10.1016/j.cma.2018.02.026>.
- [63] K. Huang, [Lectures on Statistical Physics and Protein Folding](#), WORLD SCIENTIFIC, 2005. doi: [10.1142/5741](https://doi.org/10.1142/5741).
- [64] S. Kumar, J. M. Rosenberg, D. Bouzida, R. H. Swendsen, P. A. Kollman, The weighted histogram analysis method for free-energy calculations on biomolecules. i. the method, *Journal of Computational Chemistry* 13 (8) (1992) 1011–1021.
- [65] L. Maragliano, E. Vanden-Eijnden, Single-sweep methods for free energy calculations, *The Journal of Chemical Physics* 128 (18) (2008) 184110. doi:[10.1063/1.2907241](https://doi.org/10.1063/1.2907241).
- [66] P. G. Constantine, E. Dow, Q. Wang, Active subspace methods in theory and practice: Applications to kriging surfaces, *SIAM J. Sci. Comput.* 36 (4) (2014) A1500–A1524.
- [67] W. Li, G. Lin, An adaptive importance sampling algorithm for bayesian inversion with multimodal distributions, *Journal of Computational Physics* 294 (2015) 173 – 190.
- [68] V. Vittaldev, R. P. Russell, R. Linares, Spacecraft uncertainty propagation using gaussian mixture models and polynomial chaos expansions, *Journal of Guidance, Control, and Dynamics* 39 (12) (2016) 2615–2626. doi:[10.2514/1.g001571](https://doi.org/10.2514/1.g001571).
- [69] J. Feinberg, H. P. Langtangen, Chaospy: An open source tool for designing methods of uncertainty quantification, *Journal of Computational Science* 11 (2015) 46 – 57. doi:<https://doi.org/10.1016/j.jocs.2015.08.008>.

- [70] J. Wan, N. Zabaras, A probabilistic graphical model based stochastic input model construction, *Journal of Computational Physics* 272 (2014) 664 – 685. doi:<https://doi.org/10.1016/j.jcp.2014.05.002>.
- [71] X. Wan, G. Karniadakis, Multi-element generalized polynomial chaos for arbitrary probability measures, *SIAM J. Sci. Comput.* 28 (2006) 901–928.
- [72] J. A. S. Witteveen, H. Bijl, Modeling arbitrary uncertainties using gram-schmidt polynomial chaos, in: 44th AIAA Aerospace Sciences Meeting and Exhibit, American Institute of Aeronautics and Astronautics, 2006, pp. 1706–1713. doi:[doi:10.2514/6.2006-896](https://doi.org/10.2514/6.2006-896).
- [73] M. Zheng, X. Wan, G. E. Karniadakis, Adaptive multi-element polynomial chaos with discrete measure: Algorithms and application to spdes, *Applied Numerical Mathematics* 90 (2015) 91–110.
- [74] S. Yin, D. Yu, Z. Luo, B. Xia, An arbitrary polynomial chaos expansion approach for response analysis of acoustic systems with epistemic uncertainty, *Computer Methods in Applied Mechanics and Engineering* 332 (2018) 280 – 302. doi:<https://doi.org/10.1016/j.cma.2017.12.025>.
- [75] R. Ahlfeld, B. Belkouchi, F. Montomoli, Samba: Sparse approximation of moment-based arbitrary polynomial chaos, *Journal of Computational Physics* 320 (2016) 1 – 16. doi:<https://doi.org/10.1016/j.jcp.2016.05.014>.
- [76] C. F. Dunkl, Y. Xu, *Orthogonal Polynomials of Several Variables*, 2nd Edition, Encyclopedia of Mathematics and its Applications, Cambridge University Press, 2014. doi:[10.1017/CBO9781107786134](https://doi.org/10.1017/CBO9781107786134).
- [77] E. Candès, M. Rudelson, T. Tao, R. Vershynin, Error correction via linear programming, in: 46th Annual IEEE Symposium on Foundations of Computer Science (FOCS’05), 2005, pp. 668–681.
- [78] E. J. Candès, The restricted isometry property and its implications for compressed sensing, *C. R. Acad. Sci. Paris Sér. I Math.* 346 (2008) 589–592.
- [79] M. E. Davies, R. Gribonval, Restricted isometry constants where  $\ell_p$  sparse recovery can fail for  $0 < p \leq 1$ , *IEEE Trans. Inf. Theory* 55 (2010) 2203–2214.
- [80] D. Donoho, M. Elad, V. Temlyakov, Stable recovery of sparse overcomplete representations in the presence of noise, *Information Theory, IEEE Transactions on* 52 (1) (2006) 6–18.
- [81] E. V. D. Berg, M. Friedlander, Spgl1: A solver for large-scale sparse reconstruction, <http://www.cs.ubc.ca/labs/scl/spgl>.
- [82] E. J. Candès, T. Tao, Decoding by linear programming, *IEEE Trans. Inform. Theory* 51 (2005) 4203–4215.

- [83] E. J. Candès, J. Romberg, T. Tao, Stable signal recovery from incomplete and inaccurate measurements, *Comm. Pure Appl. Math.* 56 (2006) 1207–1223.
- [84] B. K. Natarajan, Sparse approximate solutions to linear systems, *SIAM J. Sci. Comput.* 2 (1995) 227–234.
- [85] T. M. Russi, [Uncertainty Quantification with Experimental Data and Complex System Models](#), Ph.D. thesis, University of California, Berkeley (2001).
- [86] X. Yang, H. Lei, N. A. Baker, G. Lin, Enhancing sparsity of hermite polynomial expansions by iterative rotations, *J. Comput. Phys.* 307 (2016) 94 – 109.
- [87] M. Jardak, C.-H. Su, G. E. Karniadakis, Spectral polynomial chaos solutions of the stochastic advection equation, *J. Sci. Comput.* 17 (1-4) (2002) 319–338.
- [88] X. Yang, X. Wan, L. Lin, A general framework of enhancing sparsity of generalized polynomial chaos expansions (2017). [arXiv:arXiv:1707.02688](#).
- [89] A. R. Atilgan, S. R. Durell, R. L. Jernigan, M. C. Demirel, O. Keskin, I. Bahar, Anisotropy of fluctuation dynamics of proteins with an elastic network model, *Biophysical Journal* 80 (1) (2001) 505–515.
- [90] P. Ren, J. Chun, D. G. Thomas, M. J. Schnieders, M. Marucho, J. Zhang, N. A. Baker, Biomolecular electrostatics and solvation: a computational perspective, *Quarterly reviews of biophysics* 45 (4) (2012) 427–491. doi:[10.1017/S003358351200011X](https://doi.org/10.1017/S003358351200011X).
- [91] N. A. Baker, Biomolecular Applications of Poisson?Boltzmann Methods, in: K. B. Lipkowitz, R. Larter, T. R. Cundari (Eds.), *Reviews in Computational Chemistry*, John Wiley & Sons, Inc., 2005, pp. 349–379. doi:[10.1002/0471720895.ch5](https://doi.org/10.1002/0471720895.ch5).
- [92] E. Jurrus, D. Engel, K. Star, K. Monson, J. Brandi, L. E. Felberg, D. H. Brookes, L. Wilson, J. Chen, K. Liles, M. Chun, P. Li, D. W. Gohara, T. Dolinsky, R. Konecny, D. R. Koes, J. E. Nielsen, T. Head-Gordon, W. Geng, R. Krasny, G.-W. Wei, M. J. Holst, J. A. McCammon, N. A. Baker, Improvements to the APBS biomolecular solvation software suite, *Protein Science* 27 (1) (2018) 112–128. doi:[10.1002/pro.3280](https://doi.org/10.1002/pro.3280).
- [93] A. Shrake, J. Rupley, Environment and exposure to solvent of protein atoms. lysozyme and insulin, *Journal of Molecular Biology* 79 (2) (1973) 351 – 371.
- [94] M. Rasheed, N. Clement, A. Bhowmick, C. Bajaj, [Statistical Framework for Uncertainty Quantification in Computational Molecular Modeling](#), in: Proceedings of the 7th ACM International Conference on

Bioinformatics, Computational Biology, and Health Informatics, ACM, New York, NY, USA, 2016, pp. 146–155.

- [95] N. Clement, M. Rasheed, C. L. Bajaj, [Viral Capsid Assembly: A Quantified Uncertainty Approach](#), Journal of Computational Biology 25 (1) (2018) 51–71. doi:[10.1089/cmb.2017.0218](https://doi.org/10.1089/cmb.2017.0218).
- [96] H. Rauhut, Compressive sensing and structured random matrices, Radon Series Comp. Appl. Math. 9 (2010) 1–92.
- [97] A. Marrel, B. Iooss, B. Laurent, O. Roustant, [Calculations of Sobol indices for the Gaussian process metamodel](#), Reliability Engineering & System Safety 94 (3) (2009) 742 – 751.
- [98] G. Chastaing, F. Gamboa, C. Prieur, [Generalized Sobol sensitivity indices for dependent variables: numerical methods](#), Journal of Statistical Computation and Simulation 85 (7) (2015) 1306–1333. doi:[10.1080/00949655.2014.960415](https://doi.org/10.1080/00949655.2014.960415).
- [99] H. J. C. Berendsen, D. van der Spoel, R. van Drunen, GROMACS: A message-passing parallel molecular dynamics implementation, Computer Physics Communications 91 (1) (1995) 43–56. doi:[10.1016/0010-4655\(95\)00042-E](https://doi.org/10.1016/0010-4655(95)00042-E).
- [100] J. Wang, R. M. Wolf, J. W. Caldwell, P. A. Kollman, D. A. Case, Development and testing of a general amber force field, Journal of Computational Chemistry 25 (9) (2004) 1157–1174.
- [101] C. I. Bayly, P. Cieplak, W. Cornell, P. A. Kollman, A well-behaved electrostatic potential based method using charge restraints for deriving atomic charges: the resp model, The Journal of Physical Chemistry 97 (40) (1993) 10269–10280.
- [102] B. Hess, H. Bekker, J. C. Berendsen Herman, G. E. M. Fraaije Johannes, Lincs: A linear constraint solver for molecular simulations, Journal of Computational Chemistry 18 (12) (1998) 1463–1472.
- [103] W. L. Jorgensen, J. Chandrasekhar, J. D. Madura, R. W. Impey, M. L. Klein, Comparison of simple potential functions for simulating liquid water, The Journal of Chemical Physics 79 (2) (1983) 926–935.
- [104] S. Miyamoto, A. Kollman Peter, Settle: An analytical version of the shake and rattle algorithm for rigid water models, Journal of Computational Chemistry 13 (8) (2004) 952–962.
- [105] N. A. Baker, D. Sept, S. Joseph, M. J. Holst, J. A. McCammon, Electrostatics of nanosystems: application to microtubules and the ribosome, Proceedings of the National Academy of Sciences 98 (18) (2001) 10037–10041.